TITLE **Low Energy He^+ and Li^+ Ion Scattering from Surfaces**

AUTHOR Mark John Ashwin

INSTITUTION and DATE University of Warwick 1990

Low Energy He^+ and Li^+ Ion Scattering from Surfaces

by

Mark John Ashwin

A thesis submitted to the University of Warwick for admission to the degree of Doctor of Philosophy.

Department of Physics

August 1990

Contents

Acknowledgments

Many people have aided me throughout my Ph.D. studies from its beginning to its fulfilment. In particular I would like to thank

- Professor D.P.Woodruff for his guidance and assistance throughout the Ph.D. and especially for his advice in the preparation of this text.
- Mr. R.I.Johnston for his advice and invaluable technical assistance.
- Dr. M.D.Crapper for his guidance in the early years of the Ph.D. studies.
- To members, past and present, of the Surface Science group and of the Physics Department and University for their assistance and also their friendship which helped to smooth the often rough passage through the Ph.D.
- The Physics Department and the Science and Engineering Research Council for the provision of facilities and financial support to enable this Ph.D. course to proceed.
- To P.J.Thompson for his assistance in the preparation of this thesis.
- and finally but not least, my parents and family for their support throughout my academic career.

Declaration

I declare that this thesis contains an account of my research carried out in the Department of Physics at the University of Warwick between October 1985 and December 1989 under the supervision of Professor D.P.Woodruff. The computer program used for data analysis was originally written by Professor D.P.Woodruff and subsequently revised by both of us. The research described herein has not been submitted either partly or totally at this academic institution or any other for admission to a higher degree. Some parts have been published

- M.J.Ashwin and D.P.Woodruff, Elastic Scattering and Charge Exchange in He^+ Ion Scattering from Alkali Metal Overlayers, Vacuum **38** (1988) 291

- M.J.Ashwin and D.P.Woodruff, Low Energy Ion Scattering Study of the Cu(110)(2x3)–N Structure, Submitted to Surface Science for publication.

It is hoped that the work on alkali and oxygen adsorption onto Cu(110), chapters 5 and 6, will be published in the near future.

M. J Ashwin

M.J.Ashwin

Abstract

A 150° ion scattering spectrometer has been commissioned and utilized to investigate several adsorbate systems on Cu(110). Firstly, the experimental parameters were determined by using 3keV Li^+ ions in the ICISS mode to investigate the clean Cu(110) surface. The inelastic background normally observed in Li^+ ion scattering energy distributions was found to be more sensitive to the sublayer shadowing conditions than was the substrate's elastic scattering peak. Most of the observed lower layer scattering features corresponded to multiple scattering events. Using computer modelling it was deduced that for the clean Cu(110) surface the 1st to 2nd layer spacing was compressed by (8±3)%, and the 2nd to 3rd was expanded by (11±8)% compared to the bulk values.

3keV Li^+ and 2keV He^+ ions were then used to study the Cu(110)(2x1)–O and Cu(110)(2x3)–N adsorbate systems. In the former case the Li^+ data exhibited a doubling of the Cu–Cu distance in the <110> and the <211> azimuths and were found to favour a missing row type reconstruction, in which every other <100> row had been removed. In addition, $He^+ \rightarrow O$ scattering indicated that the oxygen atoms resides in the <100> long bridge site (0.0±0.2)Å above the surface. Li^+ ion scattering from the Cu(110)(2x3)–N indicated a substantial reconstruction of the surface, with an apparent reduction in the Cu–Cu spacing in the <110> azimuth and an increase in the <211> azimuth. Many of the observations are found to be quantitatively consistent, and all are qualitatively consistent, with a reconstruction in which a local Cu(100)c(2x2)–N structure is formed. Additionally, the $He^+ \rightarrow N$ scattering results favour a N adsorption site slightly above the surface.

Adsorption of Na, K and Cs onto Cu(110) at room temperature was studied using 1keV He^+ ions, 1keV Li^+ ions were used to investigate Cs adsorption. The intensity of the alkali elastic scattering signal exhibited a 'dip' with increasing alkali coverage. For lithium this was attributed to the change in the reionization probability with changes in the surface's work function. For helium this was thought to be due to changes in the neutralization mechanism within the alkali adlayer. Additionally, the alkali metal adsorbates induced an inelastic background in the He^+ ion energy distributions, and this is ascribed to changes in the neutralization probability as the ion returns through the alkali metal overlayer.

Abbreviations

AES	Auger Electron Spectroscopy
ALCISS	Alkali impact Collision Ion Scattering Spectroscopy
CAICISS	Coaxial Impact Collision Ion Scattering Spectroscopy
HEIS	High Energy Ion Scattering
ICISS	Impact Collision Ion Scattering Spectroscopy
ISS	Ion Scattering Spectroscopy
LEED	Low Energy Electron Diffraction
LEIS	Low Energy Ion Scattering
MBE	Molecular Beam Epitaxy
MEIS	Medium Energy Ion Scattering
NEXAFS	Near Edge X-Ray Absorption Fine Structure
RBS	Rutherford Backscattering Spectroscopy
SEXAFS	Surface Extended X-Ray Absorption Fine Structure
SIMS	Secondary Ion Mass Spectroscopy
UHV	Ultra High Vacuum
UPS	Ultraviolet Photoelectron Spectroscopy
VG	Vacuum Generators Ltd.
VSW	Vacuum Science Workshop

Chapter 1.
Introduction

Theoretical and experimental analyses of the bulk properties of well ordered samples rely on the three dimensional symmetry of the bulk to describe its properties, e.g. its lattice spacing or its electron density distribution. The surface represents a departure from the three dimensional to the two dimensional regime for which the bulk theory does not apply. In addition, there may be a region of transitions between the bulk structure and the surface layer which will further complicate the situation. The surface is where the sample interacts with its environment and in order to understand these interactions we need to understand what is happening in the region of the surface and what is the role of its properties, e.g. its atomic structure.

There are three main areas where interest in the surface is keenly focussed; they are in catalysis, material degradation and semiconductors [3]. In the manufacture of chemical products the processes go through many stages, each producing their own intermediates by using different catalysts under many different reaction conditions [2,5,6]. These catalysts are usually multicomponent particulate entities, with the active element being a transition metal. In addition, reaction promoters are present to enhance a particular facet of the reaction. The complex formulations used have largely been arrived at by empirical methods. Bearing in mind the size of the chemical industry, any increase in efficiency produced by an improvement in the understanding of the processes involved is of immense importance. Usually the most expensive part of the catalyst is the transition metal, e.g. platinum or rhodium, therefore an understanding of its function may lead to a reduction in costs. Properties which could be examined are whether there is a difference in the reactivity between crystal planes, what is the site of the intermediate on the surface and how is it oriented. To perform these studies it is usual in surface science to use ultra high vacuum (UHV) and single

crystal samples. This may seem far removed from the situation in a practical catalyst, but to reach the point where we can explain the reactions it is necessary to start with a simpler system, i.e. a clean, stable and characterized environment. Additionally, it reduces the number of variables involved. From this point the fundamentals of molecular adsorption and the enhancement caused by promoters can be examined to form a database from which to build.

Material degradation is a constant threat to the integrity of materials, [3]. It can take many forms such as the formation of oxides, e.g. rust, or the diffusion of alloy components to a fault plane or the surface. In this area the process maybe internal as well as external to the material, but surface science can again help to pin point the driving forces behind these processes, by for example, examining what effect the density of steps on a surface has on the diffusion of atoms or the reactivity of a surface to an oxidant. Perhaps, one of the areas where surface studies are most important is in the semiconductor industry, especially as the integrated devices are becoming thinner and tending towards monolayer thicknesses, [3,9,10,11]. Here, the quest to design ever more novel devices and use of higher component densities on semiconductor material has driven the need for better defined multilayer semiconductors using single crystal substrates. Hence, there is a need to determine surface registry and the structure of each new layer as it is formed into a multilayer sandwich. A vital feature controlling the operation of a device is the electronic structure and how it varies with the layer composition and dimension. In the future, devices will approach the dimensions where quantum effects become significant, such as in the quantum transistor [4], and a knowledge of the electron density becomes critical in the design of such devices. In addition there are many other areas of interest, such as the magnetic properties of thin films, important for storage media, or coatings to prevent corrosion.

For a long time the properties of surfaces have been investigated, ever since Benjamin Franklin poured oil on Clapham pond [1]. The effect of the surface layer on observed properties has been postulated since the early 19th century [1]. The field received a large impetus due to the pioneering research of I. Langmuir who introduced

many concepts required by later surface investigations. He is best known for his work with K. Blogget on the two dimensional properties of monolayer films, [1]. For this and other contributions he received the Nobel prize for Chemistry in 1932. Surface studies continued through the 20th century, with discoveries such as Low Energy Electron Diffraction by Davisson and Germer (1927), [17], or Auger electron transitions by P. Auger (1925), [8,16], bulk Extended X-ray Absorption Fine Structure (EXAFS) leading to Surface-Extended X-ray Absorption Fine Structure (SEXAFS), [12]. The pace of investigation took a large up turn with the ability to obtain routinely ultra high vacuum, $<10^{-9}$ mbar in the mid sixties.

The use of ions as a surface probe is just one of the many available, but it provides a wide range of energies and the ability to perform compositional and structural information from essentially the same equipment. The range of energies used by ion scattering are usually divided into three parts, Low Energy Ion Scattering (LEIS, energies 500eV–10keV), Medium Energy Ion Scattering (MEIS, 10–600keV) and High Energy Ion Scattering (HEIS, >1MeV); these definitions are by no means rigid. One of the earliest studies of ion surface interactions was performed by Grove in 1852 [13], who investigated the sputtering of a surface by ions. Ion scattering studies did not become prevalent until the early nineteen fifties and concentrated mainly in the HEIS region of energies. In these studies a two body collision model was tested and found to be applicable and eventually led to the development of Rutherford Backscattering (RBS). In addition, the sputter products of the surface were mass analysed to determine the surface elemental composition, which latter developed into Secondary Ion Mass Spectrometry (SIMS). The extension of the energy range towards lower energies was performed in the late nineteen fifties by Brunnee [14], who found the maximum energy of the scattered ions corresponded to the classical binary collision model prediction (see chapter 2). This area of study was further developed by D.P. Smith [14] at the 3M company in the nineteen sixties, who applied the method to the analysis of elemental composition in the outermost monolayer; this led to a rapid increase in the number of ion scattering investigations. At present there is active

research into many aspects of ion scattering, such as the neutralization of ions and the effects of different work functions [15], or the determination of the universal scattering potential [20], as well as considerable interest in its application to the deduction of surface structures.

In this project ion scattering was used to try to determine the structure of the clean Cu(110) surface and the reconstructions induced in it by various adsorbates, as well as the effect of changing work functions and of a molecular adsorbate. In this investigation two ions were used, namely helium and lithium. The former suffers from a high rate of neutralization which is trajectory dependent, and is not usually considered suitable for structural analysis, though Aono has been successful, [18,19]. Lithium, on the other hand does not suffer from trajectory dependent neutralization. A particular specialization of ion scattering was used in this project, namely Impact Collision Ion Scattering Spectroscopy (ICISS), first proposed by Aono in 1981 [18].

The first part of the thesis describes the techniques that were utilized in this project. At first the project concentrated on determining the structure of the clean Cu(110) surface and understanding the scattering events taking place. Due to our choice of scattering angle, ≈150°, there were many complications that had not been foreseen, which are discussed in chapter 4. The technique was then applied to an extensively studied adsorbate structure, namely Cu(110)(2x1)-O. Here, the reconstruction is widely believed to be a missing row type structure, with the oxygen atoms occupying the <100> long bridge sites, but the O–Cu top layer spacing has proved controversial, with a large spread of values having been reported by other groups. Helium ion scattering was also used to investigate the position of the adsorbed oxygen atoms, since lithium ion scattering proves insensitive to low atomic number adsorbates. An element that is a neighbour of oxygen in the periodic table is nitrogen, but molecular nitrogen does not react with copper. An atomic adsorption structure can be formed, however, using an ion gun, and a (2x3) phase is produced, which has been studied by a few groups. Both the substrate structure and the nitrogen site have been investigated, using both lithium and helium ions. Due to the limited amount of prior

research that has been performed on this system, these aspects of the system are still the subject of debate within surface science. The results presented indicate that a large reconstruction has taken place within the surface layer. The final experimental chapter is an investigation of the application of ICISS to a very different adsorbate. It is known that a small amount of alkali metal adsorption produces large changes in the work function of surfaces (and indeed in some f.c.c. (110) surfaces causes a (1x2) surface reconstruction). We find that this appears to produce significant changes in the ion scattering yield of helium and find evidence of significant associated charge exchange phenomena. Some final comments on the project are presented in chapter 7.

1.1. References

1. A. Zangwill, Physics at a Surface. Cambridge University Press 1988
2. R.P.H. Gasser, An Introduction to Chemisorption and Catalysis by Metals. Oxford Science Publications 1985
3. D.P. Woodruff and T.A. Delchar, Modern techniques of Surface Science. Cambridge Solid State Series 1986
4. R.T. Bate, Scientific American **258** (1988) 78
5. M.Bowker and R.J Joiner, Physics World March (1989) 35
6. M. Chesters, Physics World March (1989) 40
7. D.A. King , Physics World March (1989) 45
8. R.Sietmann, Physics Bulletin **39** No.8 (1988) 316
9. G.Davies, Physics Bulletin **39** No.9 (1988) 22
10. L. Eaves and G. Toombs, Physics Bulletin **39** No.9 (1988) 24
11. G. Rees, Physics Bulletin **39** No.9 (1988) 26
12. J. Stohr , X-Ray Adsorption: Principles, Techniques and Applications of EXAFS, SEXAFS and XANES. Eds R.Prins and D.C. Kronigsberger (Wiley, New York, 1988)
13. G.M. McCraken, Rept. Prog. Phys. **38** (1975) 261
14. D.P. Smith, Journ. Appl. Phys. **38** (1967) 340
15. M. Aono, Nucl. Instr. and Meths. **B27** (1987) 35
16. P. Auger, J. Phys. Radium. **6** (1925) 205
17. C.J. Davisson and L.H. Germer Nature **119** (1927) 558
18. M. Aono, Jap. Journ. of App. Phys. **20** (1981) L829
19. M. Aono, Nucl. Instr. and Meths. **B2** (1984) 374
20. O.S. Oen, Surface Science Letts. **131** (1983) L1407

Chapter 2.
Surface Science Techniques

This chapter provides a brief introduction to the techniques used within this project, with emphasis on ion scattering.

2.1. Low Energy Electron Diffraction (LEED)

LEED has become one of the standard techniques in surface science, and has been used to determine many structures, e.g. [1,2,3,12]. The first LEED experiment was performed by Davisson and Germer [5], and this and work by Thompson and Reid, [4], provided experimental evidence for wave particle duality. Until the early sixties very little surface science was performed with LEED due to the inability to obtain UHV easily.

In LEED a monoenergetic electron beam in the energy range 30–300eV is incident onto a sample from which the electrons are then scattered. An instrumental schematic is presented in figure 2.1. A typical energy spectrum of these scattered electrons is outlined in figure 2.2. The major peak at the highest energies is due to the elastically scattered electrons and these are the ones detected in LEED. At lower electron energies there is a distribution of inelastic and secondary electrons, and within this region there are peaks due to Auger electron transitions, see section 2.2. The selection of the elastically scattered electrons is accomplished by the use of three or four high transmission grids to form a high pass-filter, and a fluorescent screen, figure 2.1. To provide a field free region the first grid is fixed at earth potential. The detection of only the elastically scattered electrons is accomplished by setting the centre grids at a potential just below the primary energy of the electron beam. The elastically scattered electrons penetrating beyond these grids will have a kinetic energy of a few eV, and are then excited to their original energy by the final grid, but this is

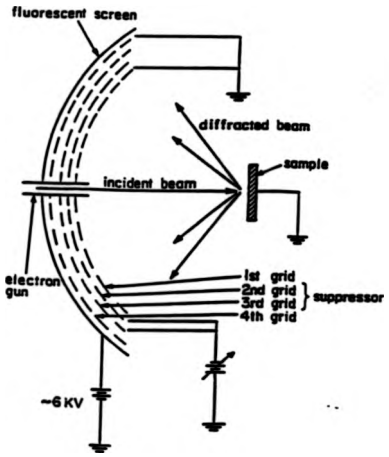

Figure 2.1 Experimental arrangement for a Low Energy Electron Diffraction (LEED) experiment using a four grid system. The sample's surface is positioned at the center of curvature of the grids and fluorescent screen. (M.A.Van Hove, W.H. Weinberg and C.M. Chan; Low Energy Electron Diffraction, Springer–Verlag Berlin Heidelberg (1986)).

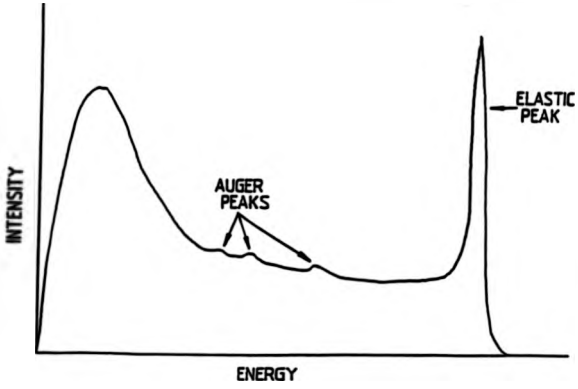

Figure 2.2 A schematic of a typical electron energy distribution curve.

insufficient to excite the phosphor on the fluorescent screen. Hence, the screen is raised to a potential of several kV to accelerate these electrons. It can be shown that the elastically scattered electrons are scattered in well defined directions depending on the crystal structure of the sample due to wave interference phenomenon as in x-ray diffraction, [6,7,8,9]. To determine the surface structure, the electrons detected need to have originated only from the surface region. If the inelastic scattering mean free path of the electrons is plotted as a function of incident electron energy, figure 2.3, it can be seen there exists a minimum in the mean free path at an incident energy of approximately 60eV of about 5Å. This can be related to the depth of penetration for the detection of elastically scattered electrons. Hence, to maximize surface sensitivity the incident electron energy in a LEED experiment is usually operated in this region, with energies ranging from 30eV to 300eV [7,10].

In a LEED experiment a series of diffracted beams may be observed on the screen for a well ordered sample. The spacing of these beams is proportional to the surface reciprocal net vectors [6,7,11,40]. This means that one can define the reciprocal lattice and hence deduce the real space lattice (Pendry [6]). Usually LEED is used as a routine test for well ordered samples, and in order to orientate the sample. This latter use proved particularly valuable in this project.

2.2. Auger Electron Spectroscopy

The technique of Auger Electron Spectroscopy provides information concerning the elemental surface concentration. This information is obtained by monitoring a particular electronic transition involving three electronic energy levels, figure 2.4, discovered by P.Auger and co-worker [13] and is known as an Auger transition. Firstly, a vacancy is created in a core energy level by photon or electron ionization, which is then filled by a more shallowly bound electron. This can result in one of two processes happening, resulting in either an electron or a photon being emitted. In an Auger transition, one electron from a higher electron level fills the vacancy and at the same time another electron is emitted with the excess energy. This results in an

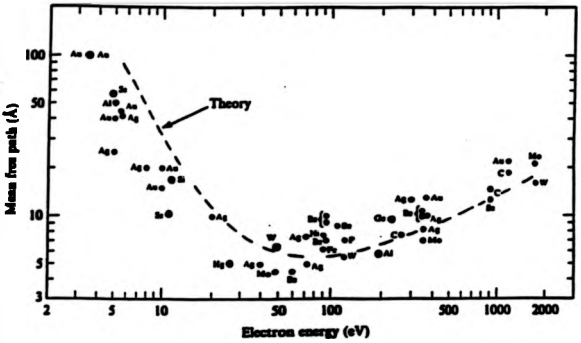

Figure 2.3 A plot of the inelastic scattering mean free path of electrons with incident kinetic energy. A minimum exists at around a kinetic energy of 60eV. (G.A.Somorjai, Principles of Surface Chemistry. Prentice-Hall Inc. (1972))

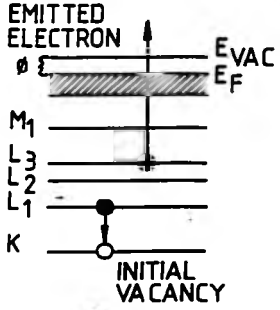

Figure 2.4 An outline of the Auger electron emission process for arbitrary electron levels.

electron being emitted whose energy is characteristic of the energy levels involved, and leaves behind an ion with two electron vacancies. Since the energy levels are characteristic of the emitting atom the energy of these Auger electrons can be used to determine the elements that are present on the surface. These electron energies have been tabulated for most elements [14]. Elements with less than four electrons cannot, of course, undergo an Auger transition. For elements up to an atomic number of 30 the Auger process dominates over the radiative processes even for the deepest energy levels, figure 2.5, [9,16].

The labelling of the individual Auger process is depicted in figure 2.6. The first letter denotes the vacancy level, and the second and third letters denote the level from which the electron which fills the vacancy originates and the level from which the Auger electron is emitted. With a knowledge of the energy levels involved in the transition the kinetic energy of the Auger electron can be calculated :

$$E_k = E_1 - E_2 - E_3 \qquad (1)$$

where

E_k = The final kinetic energy
E_1 = Initial vacancy energy level
E_2 = Energy level for vacancy filling electron
E_3 = Emitted electron's energy level

The kinetic energy deduced in this way will not be totally accurate if the neutral atom's binding energies are used, since the final state has two holes which will result in electronic rearrangement, [16,43]. In addition both the initial and the final state energy are also sensitive to the chemical (electronic) environment, [16,17]. Consequently, there are small energy shifts associated with the different environments.

The Auger transitions manifest themselves as peaks in the electron energy distribution, see figure 2.2. These Auger features, in the electron energy distribution, typically have a poor signal to background ratio, which mitigated against the use

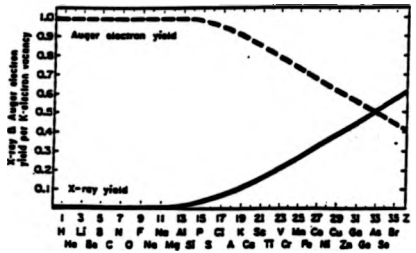

Figure 2.5 An excited electron may lose energy by non radiative or radiative processes. The yield of these two processes varies with atomic number, with the former being dominate upto an atomic number of approximately 30 and is shown schematically in this diagram. (G.A. Somorjai, Principles of Surface Chemistry. Prentice-Hall Inc. (1972))

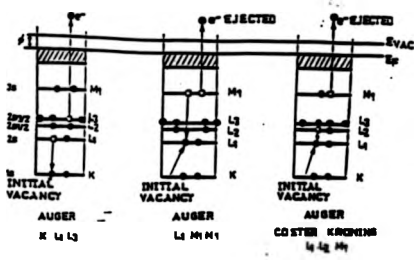

Figure 2.6 The labelling of Auger processes refers to the energy levels involved in the process. (J.Alvarez and M.C.Asensio, In Methods of Surface Analysis, Part A. Ed. J.L.Fierro Elsevier amsterdam (1989))

Auger spectroscopy for elemental analysis initially. The technique languished until L.A. Harris [17] demonstrated that the peaks could be made more distinguishable by differentiating the electron distribution spectrum, figure 2.7. The prominence of the technique was further enhanced when it was shown that a normal LEED optics could be used for Auger electron spectroscopy (AES) [18]. To obtain the best result from Auger electron spectroscopy, however, it is better to carry it out with true dispersive analysers, such as the Cylindrical Mirror Analyser (CMA) [16,20], figure 2.8, or as in this project a Concentric Hemispherical Analyser.

In addition to providing elemental identification, the concentration of an element can be quantified [43]. In particular, if the growth mode of an adsorbate is layer by layer, the so called Frank-van der Merwe growth mode, the intensity of the Auger electron flux will exhibit a linear relationship with elemental concentration up to monolayer coverage [12,16,19,43]. The linearity of the signal may also exhibit changes in gradient on completion of a monolayer and still maintain a local linear relationship [16,19,43], figure 2.9. Accurate determination of the concentrations of the elements present can be determined provided the dependence of the Auger electron intensities on elemental concentration are calibrated. Hence, Auger electron spectroscopy provides a means of identifying and quantifying the elemental composition of a surface.

2.3. Introduction to Ion Scattering

2.3.1. Binary Collision Model

When a particle, such as an atom or an ion, scatters off a crystal the resulting backscattered flux is a mixture of particles in varying charge states and possessing a variety of kinetic energies. This backscattered flux contains information concerning the type of scattering events that have taken place. To extract the information carried in this flux a theoretical model to describe the situation is needed. One explanation of a particular scattering event can be obtained, by the application of the classical binary

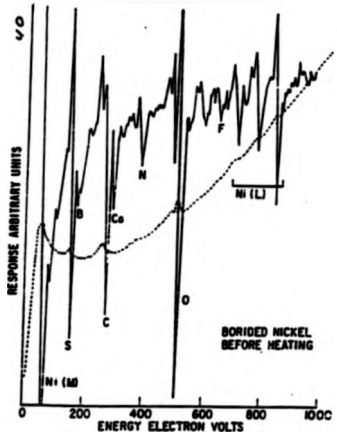

Figure 2.7 An illustration of the enhancement of the Auger transition peaks compared to the electron background obtained by the use of differentiation of an electron energy spectra. The dashed line is the direct response (N(E)) and the full line the amplified differential response (d N(E)/dE) (L.Harris, J. Appl. Phys. **39** (1968) 1419)

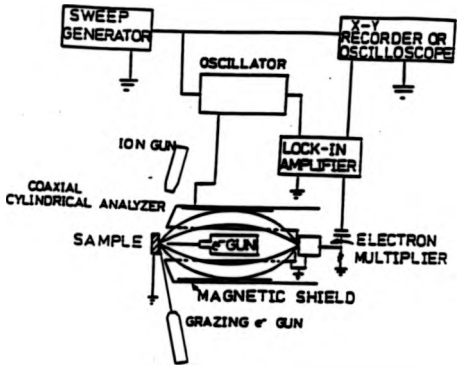

Figure 2.8 One typical experimental arrangement to obtain the differentiation of an electron energy distribution curve. (J.Alvarez and M.C. Asensio, In methods of Surface Analysis, Part A. Ed. J.L.Fierro Elsevier Amsterdam (1989))

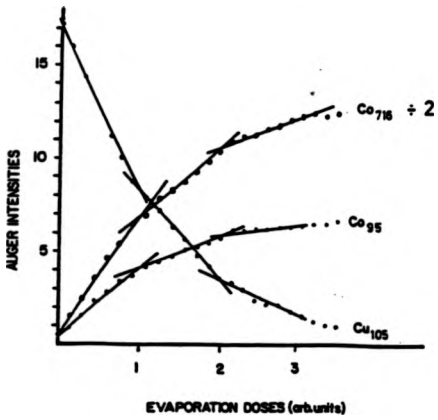

Figure 2.9 The intensity of an Auger peak exhibits a linear increase with elemental concentration with changes in gradient at the completion of each layer, for a layer by layer growth mode. (L.Gonzalez et al., Phys. Rev. **B24** (1981) 3245

collision model. The scattering conditions for which the binary collision model is obtained are depicted in figure 2.10. In this an atom of mass m_1 is moving towards an unbound isolated, stationary atom of mass m_2; the incoming atom then scatters off the stationary atom in a particular direction. The mathematical derivation is carried out in appendix A, [84]. By applying energy and momentum conservation, and ignoring inelastic losses, the following equation can be obtained :-

$$\frac{E_1}{E_2} = [1+A]^{-2} [\, \text{Cos}\, \theta_1 \pm (A^2 - \text{Sin}^2\, \theta_1)^{1/2} \,]^2 \qquad (1)$$

where

E_1 = Energy of the backscattered atom

E_2 = Energy of the Incident Atom

A = Ratio of the target mass to the incident atom mass

θ_1 = Total scattering angle

For this model to be applied to ion scattering there are three assumptions being made. The first is that the scattering atom in the crystal behaves as though it is unbound, i.e. like a gas atom. This requires that the effects due to the lattice are negligible during the scattering event; if they are not, the effective mass of the scattering atom will be modified since it is more strongly constrained than the free gas atom. This increase in effective mass would produce scattered ions with greater than expected kinetic energies. The second assumption is that the target atom is essentially stationary; this is expected to be valid since the velocity of the scattering atom is small in comparison with the scattered incident particle [86]. Hence the incoming atom will see a stationary lattice; also the energy associated with the lattice vibration is negligible compared to that of the scattering particle. The final assumption is that the energy losses occurring during the scattering events are entirely kinetic. This requires that the inelastic and electronic interaction energy losses are small compared to the elastic energy loss in the scattering event.

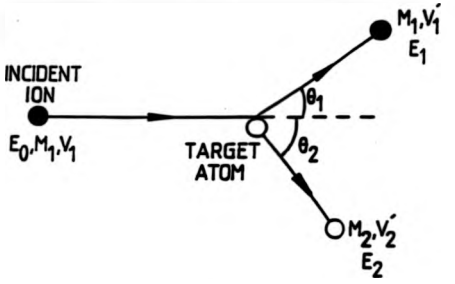

Figure 2.10 The scattering event utilized for determining theoretically the energy transfers during a binary collision, is depicted here and attributes the symbols used to the relevant particles.

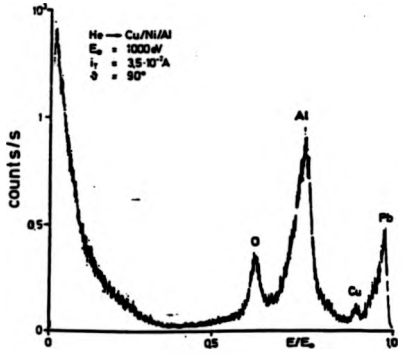

Figure 2.11 An energy distribution for helium ion scattering from a multi elemental sample. (E.Taglauer and W.Heiland, App. Phys. 9 (1976) 261)

Historically, scattering reactions were first investigated using high energy projectiles, for example Li^+, H^+ and He^+, with energies of several MeV. It was noticed by Rubin that peaks in his energy distribution spectra, a plot of intensity versus ion energy, could be explained by using the classical binary collision model [85]. Other researchers observed that for H^+ and He^+, which have a large inelastically scattered ion background, the maximum energy of the backscattered ions could also be explained with the same model. These peaks or maximum energy thresholds can be related to a particular scattering element, and this then offered the possibility of precise elemental determination using well understood classical physics [87]. In addition, the scattering cross-section of any of the ion atom combinations could be calculated from first principles, and were found to be in good agreement with experiment. At these energies the scattering cross-sections are small ($\approx 0.1 Å^2$ [22]) leading to substantial ion beam penetration. Hence this technique is insensitive to the surface, due to the surface information being obscured by the large bulk contribution to the data.

There are two different methods that can be employed to limit the contribution of scattering from the bulk. For HEIS one method is to choose a particular (crystallographic axis) incident direction, where the atoms align in parallel rows. In this geometry the substrate atoms are shadowed by those close to the surface and the scattering signal becomes sensitive to any small atomic misalignment. These are known to exist between the surface and the bulk, but the ability to detect these effects relies on the small scattering cross-sections [15]. The choice of the angle of incidence does rely, of course, on a knowledge of the bulk structure, but this is readily availible from x-ray diffraction. Additionally, the enhanced surface sensitivity and well known cross–sections allow the determination of elemental concentrations. A disadvantage of this method is that specific crystallographic directions have to be used. Also, it is not sensitive to low Z adsorbates on the surface, due to their relatively small scattering signals since the scattering signal is proportional to the scattering cross–section which is proportional to Z^2. An alternative method of improving the surface sensitivity of the

incident particles is to reduce the kinetic energy of the incident ions, thereby increasing the scattering cross-sections, which then reduces the penetration of the ion beam. This decrease in the energy of the ions then increases the time ions are in the vicinity of the surface. Since there is now an increase in the collision time, it was not known if the binary collision model predictions would correspond to the scattering peaks at these lower energies. Research was carried out in this area by various researchers, [87,89,90,91,92]. These experiments utilized ions with energies ranging from 0.4 keV to 100 keV, and it was found that the binary collision model was valid over this energy range.

The validity of this model has been found to hold for ion energies greater than 400eV upwards. Below approximately 200eV Hulkpe [93] discovered deviations from the binary collision approximation. When examining equation 1, it can be seen that there is the possibility for two values of the energy ratio to be obtained for a particular set of conditions, due to the ambiguity of sign of the square root. From the theory in appendix A it can be deduced that for values of the mass ratio, A, greater than 1 it is only a single valued function; for A less than 1, two values for the energy ratio will be obtained. The prediction of two values indicates that there would be two peaks in the energy distribution due to scattering off the same atom. The validity of the double valued case has been established by experiment, for example [94]. The results of the binary collision model suggest that by analysing the energies of the backscattered ions the identity of the scattering atoms can be identified. Thus, in principle this provides a method for mass analysing the sample without having to destroy it. There are however, a few points to be considered before the technique can be applied. For instance, how well resolved are the peaks, what are their intensities, and what effect does the mass of the incident ion have? These are important points if the elements within the sample are to be accurately determined.

To identify the elements which are present in the sample the ions have to be energy analysed and the result presented as an intensity versus energy diagram, an example of which is given in figure 2.11. To simplify the analysis the value of A

should be chosen to be greater than one, which reduces the number of peaks to one for each element, provided only singly charged ions are detected, as is found experimentally. To obtain a value for A of greater than one for the lightest adsorbate, it is necessary to use incident ions such as helium, hydrogen or lithium; this reduces the number of peaks, but degrades the mass resolution of the spectrum. The energy resolution of the spectrum is a function of the analyser the incident ion beam energy spread and the angular acceptance of the analyser. Setting the energy resolving power to fixed value and using the binary collision model an expression for the mass resolving power can be determined to be (see appendix C and [86]):-

$$\frac{M_2}{\Delta M_2} = \frac{E_1}{\Delta E_1} \cdot \frac{2A}{(A+1)} \cdot \frac{A+\mathrm{Sin}^2\theta_1 - \mathrm{Cos}\,\theta_1(A^2-\mathrm{Sin}^2\theta_1)^{1/2}}{(A^2-\mathrm{Sin}^2\theta_1+\mathrm{Cos}\,\theta_1(A^2-\mathrm{Sin}^2\theta_1)^{1/2})} \qquad (2)$$

where

ΔM_2= Mass resolution of the spectrum for the target mass

ΔE_1 = Energy resolution of the instrument

The mass resolving power of the spectrum therefore depends on the scattering angle, mass ratio and the backscattered ion energy. It is linearly dependent on the energy of the backscattered ion energy, and therefore the mass resolving power increases with increasing ion energy for a fixed energy resolution. Hence, the peaks in a given energy distributions should become sharper the larger their energy. The easiest method to visualize the effect of the other variables on the mass resolving power is to employ a graphical method. In figure 2.12 the mass resolving power is plotted as a function of incident ion mass; a further point to note, is that the mass resolving power increases for a particular atom's mass with increasing incident ion mass. These facts suggest that the method of obtaining greater mass resolution is to employ larger incident ion masses. Also, to maintain the one peak per element present means there is an upper limit placed on the incident ion mass, imposed by this condition. The decrease in the gradient with increasing target mass indicates that the resolution of the peak for the larger masses is asymptotic. A variable related to these effects is the

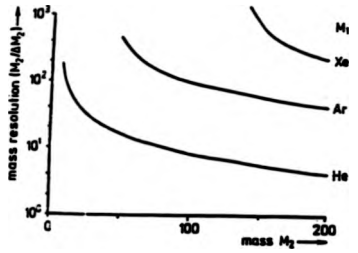

Figure 2.12 The variation of mass resolution for various incident ions with increasing target mass. (E.Taglauer and W.Heiland, App. Phys. **9** (1976) 261)

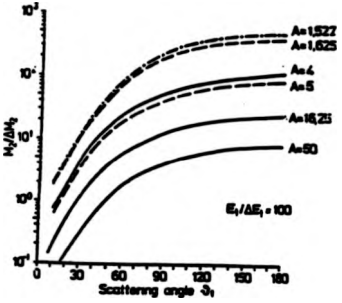

Figure 2.13 The variation of mass resolution for several ratios of target mass to ion mass with increasing total scattering angle. (E.Taglauer and W.Heiland, App. Phys. **9** (1976) 261)

variation in mass resolving power with the scattering angle for different mass ratios, figure 2.13. If the mass ratio is decreased for a given scattering angle, the mass resolving power increases, this implies that the closer the ion and atom are in mass the better the mass resolution. This set of conditions also exhibits an asymptotic relationship, in this case the change in mass resolving power is decreasing with increasing scattering angle. We therefore have a choice as to whether to use a heavier ion or a large scattering angle. The advantage of using a large scattering angle is that the change in mass resolving power is small as a function of the scattering angle; therefore the resolving power is constant for the whole of the acceptance angle of the analyser, providing it is not too large.

Up to this point the discussion has concentrated on the scattered ion, the other part of this interaction is the effect on the target atom. Of importance is the amount of energy the scattering atom receives and what happens to it after the collision. To obtain a first approximation of the event the binary collision model can be used, it will only describe its initial reaction due to the effects of atomic bonding afterwards. The model is applied to the target atom; from this ratio of the target atom energy (E_2) to the energy of the incident ion (E_0) is given by :-

$$\frac{E_2}{E_o} = \frac{4A}{(1+A)^2} \cdot \cos^2\theta_2 \qquad (3)$$

See appendix B for the derivation.

This equation is a single valued function, in contrast to the scattered ion equation (1) and indicates the amount of energy deposited in the sample. The strength of the atomic bonding has not been taken into account, and this will affect the final trajectory that the target atom follows after the collision. The energy deposited will not be entirely retained by the atom, it will be communicated to the other members of the lattice. As a result an atom may even escape the surface, i.e. sputtered. This requires at least two atoms to reverse the initial recoil direction, since the reaction provides momentum directed into the sample. The sputtering has been investigated by several

researchers [88,94,95,96].

2.3.2. Shadow Cones and Potentials

Using the preceding theory it is clear that if the energy of the scattered ion can be determined for a particular set of experimental conditions, the scattering atom's identity can be established. However, this will not provide information on the spatial distribution of the atoms. This information is obtained as a result of the phenomenon of shadowing. If the trajectories of all possible incident ions are examined it is found that there exsists a region behind the scattering atom into which no ions penetrate, figure 2.14, [27,28,43]. If another atom is situated in this region it will not be 'seen' by the incoming ion flux, i.e. it is shadowed. For low energy ion scattering the width of the shadow cones is of the order of Å's, hence, it is comparable with the interatomic spacings for crystals. The shadow cone then obscures a large proportion of the lower atomic layers of the crystal. Note that if the edge of the shadow cone is examined, it can be seen that there is an increased flux density compared with the incident density. This "focussing" at the edge of the shadow cone is important in the determination of surface structure, and will be discussed later. In order to calculate the trajectories qualitatively an expression for the interaction potential is required.

The interaction potential has to take account of a large number of variables. This is because the two interacting particles are not single entities, but they consist of nuclei and electrons. Therefore, the potential has to include contributions from the electron–electron, electron–nuclei and nuclei–nuclei interactions. To a good approximation we need only consider coulombic interactions and then an expression of the form is obtained:-

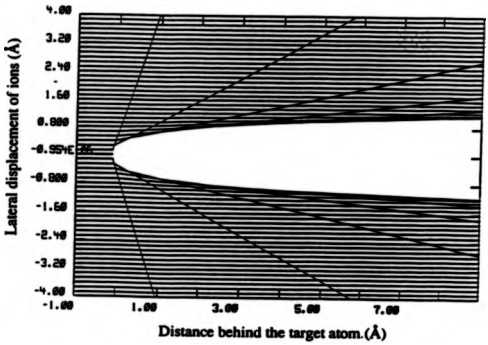

Figure 2.14 Scattering trajectories for 1 keV He^+ scattering from a copper atom, assuming a Thomas Fermi Molière potential with a screening parameter of 0.65.

$$V = \frac{1}{2}\sum_{\substack{i,j \\ i\neq j}}^{n} \frac{e^2}{4\pi\varepsilon_o r_{ij}} - \sum_{i}^{n} \frac{Z_1 e^2}{4\pi\varepsilon_o r_i} + \sum_{j}^{n} \frac{Z_2 e^2}{4\pi\varepsilon_o r_j} + \frac{Z_1 Z_2 e^2}{4\pi\varepsilon_o r_{12}} \qquad (4)$$

electron/ electron	electron / nuclei 2	electron / nuclei 1	nuclei 1/ nuclei 2

This is quite a complex equation, and requires many assumptions in order to utilize it. In high energy Rutherford Backscattering the usual form of the potential is the Coulombic internuclear potential only, the electronic contributions being negligible. An indication of how close the ions approach the scattering atom can be obtained by equating the potential energy to the kinetic energy, see L.C. Feldman [42].

i.e.

$$E = \frac{Z_1 Z_2 e^2}{d\,(4\pi\,\varepsilon_o)} \qquad (5)$$

from which:–

$$d = \frac{Z_1 Z_2 e^2}{E\,(4\pi\,\varepsilon_o)} \qquad (6)$$

where

E = Kinetic Energy of the Incident Ion

Z_1 = Ion's atomic number

Z_2 = Atom's atomic number

e = Electronic charge

d = Distance between the ion and the atom

Therefore for a 1 MeV helium scattering off a copper target atom, has a distance of closest approach of ≈8.3×10^{-4}Å. In comparison the first Bohr radius is ≈0.53Å, therefore in the Rutherford backscattering regime, the ion penetrates deep inside the

electron cloud and sees an unscreened nucleus at its closest approach. This then allows the use of pure nuclear coulombic repulsion for the potential. In comparison, taking the energy as 1keV leads to a distance of closest approach of ≈0.83Å. In this case the ion perihelion is in amongst the orbital electrons, which indicates that the electronic contribution will be more significant. The potential in equation 4 includes these interactions, but this many electron potential cannot be evaluated.

In describing the scattering of the low energy ions several appropriate potentials have been developed and utilized. In this energy range there has to be an allowance for the screening of the nuclear charge by the electrons. The potentials are semi-empirical in nature, with the initial theory being refined by comparison with experimental data, due to the uncertainty concerning the description of the multi component interactions which take place. Potentials that have been used are the Morse, Born-Mayer, Thomas-Fermi, Gibson, Bohr and others, [23,24,25,29,30,34,38, 40]. There has been an attempt also to produce a universal potential to cover the low and the high energy ranges (0.1keV - 1MeV) of the incident ions, Oens [26]. In the empirical derivations the simplest assumption is to consider the atom as a hard sphere potential with infinite height within the defined radius. A more refined approach is to include a short range attractive force. This approach has been used in the Lennard-Jones and the Morse potentials [38]. These potentials were used in the early days of ion and atom scattering and are applied at the present. Another potential that has been used was the Born-Mayer potential [25,34,38]. This is based on an exponential decay function of the form :-

$$V(r) = A\, e^{-Br} \qquad (7)$$

where A and B are the adjustable parameters, and were adjusted to agree with experimental data. This was first proposed by Born and Mayer in 1932 to describe the interatomic potentials in ionic crystals. The potential becomes less accurate for small distances of separation – values for the two constants have been tabulated for various atom pairs by Abrahamson 1969 [97]. The virtue of this potential is its simplicity and

that it is able to describe the scattering events particularly for low energies. It has been revised by Huntingdon and Gibson to reduce its essentially infinite range to the order of the lattice spacing of crystals, [33]. W.I. Gray et al. [36], have studied its accuracy over the energy range 25eV to 10keV. They carried out the investigations on a computer for various crystal structures, and it was found that the results obtained agreed with the predictions of the binary collision model for scattering events. However, the Born-Mayer potential has largely been supplanted by the Thomas-Fermi (TF) potential in recent years, [24,28]. This belongs to another group of potentials which are based on a screened Coulomb potential and are of the form:-

$$V(r) = \frac{Z_1 Z_2 e^2}{4\pi \varepsilon_o r} \chi(r) \qquad (8)$$

where $\chi(r)$ = The screening function

One of the simplest screening functions was proposed by Bohr, and utilized an exponential function for the screening function. The TF potential was proposed at approximately the same time and was originally developed for the interatomic potentials in crystals, was based on TF statistics [40], and was first developed for one atom. This potential has its limitations, in that it was found to be too soft at short interatomic distance and too hard at large distances. These inaccuracies could be partly attributed to the lack of incorporation of the influence of electronic exchanges. This was addressed in further developments, the two main variations are the Thomas-Fermi-Dirac (TFD) and the Thomas-Fermi-Firsov approximations. It is the latter which forms the basis of most low energy ion scattering calculations, including those in this thesis. Firsov [24] derived the limits of accuracy of his potential and concluded that the model became invalid for separations greater than approximately 1Å, due to its statistical nature. The potential is of the form :-

$$U(r) = \frac{Z_1 Z_2 e^2}{4\pi \varepsilon_0 r} \cdot \chi\left(\left[Z_1^{1/2} + Z_2^{1/2} \right]^{3/2} r/a \right) \qquad (9)$$

where $\chi(r)$ is a screening function

a = screening length

The form of the screening function used in this research is due to Moliere [28,43] and is used in the majority of ion scattering simulations at the present. The potential then has the form :-

$$U(r) = \frac{Z_1 Z_2 e^2}{4\pi \varepsilon_0 r} \cdot \chi(r/a) \qquad (10)$$

and the screening function is given by :-

$$\chi(x) = 0.35 \exp(-0.3x) + 0.55 \exp(-1.2x) + 0.1 \exp(-6.0x) \qquad (11)$$

where x = (r/a C)

For the Firsov approximation $a = 0.4685 \left(Z_1^{1/2} + Z_2^{1/2} \right)^{-2/3}$ (12)

C is an adjustable parameter, and is adjusted by comparison with experiments.

As has already been mentioned, there is a region of space in which incident ions do not enter, known as the shadow cone. A useful variable to deduce is the width of the shadow cone for different distances behind the shadowing atom. This will also provide an indication of the area of the crystal shadowed. The behaviour of the shadow cone can be derived numerically using a useful result from classical theory. If the potential is considered to be spherically symmetric, then an expression for the total scattering angle of the ion can be deduced :-

$$\theta_{cm} = \pi - \int_0^{\infty} \frac{2\, b\, dr}{r^2 \left(1 - \left(b^2/r^2 \right) + \left(V(r)/E \right)^{1/2} \right.} \qquad (13)$$

where

b = Impact parameter

E = Kinetic Energy of the incident ion

θ_{cm} = Total scattering angle in the center of mass frame.

The total scattering angle obtain from this equation needs to be converted to the laboratory frame of reference, before it can be used to plot trajectories. A shadow cone is depicted for 1keV helium in figure 2.14. Using this equation a relationship for the shadow cone width has been derived by Martynenko [98] and also by Oens [26].

2.3.3. Neutralization

When an ion approaches a surface electron exchange can occur between its filled and partially filled and empty electron orbitals, and those of the surface. The complex interaction of the orbitals will determine the final charge state of the ion. This interaction has been the subject of intense investigation from the earliest days of ion scattering [45,46,47]. At present research is proceeding on experimental and theoretical fronts. Experimental work is mainly concerned with the determination of the emergent charge fractions, and the effects of the presence of adsorbates [51–83,99].

A neutral atom can be produced by several different electronic interactions, each having its own probability of occurrence. Usually, there are considered to be only four types of interaction and these are depicted in figure 2.15. In these diagrams the ion's energy levels are depicted on the right and the surface's conduction band on the left- in

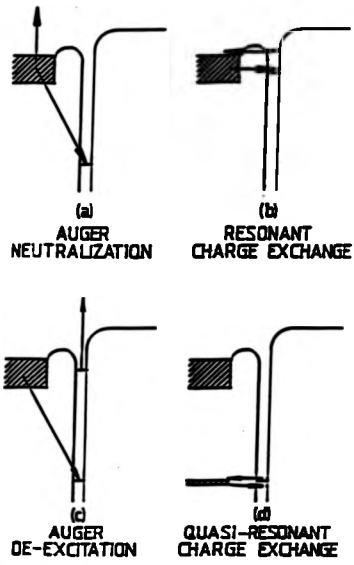

Figure 2.16 The possible electron processes between the incoming ion and the target metal surface. The surface's conduction band is situated on the left and the incoming ion is on the right.

figure 2.15 this is assumed to be a metal. All of these processes are still available to semiconductors and insulators. In these schematic diagrams there is no explicit indication of the distance between the ion and the atom. These charge exchange processes have no definite range, but according to quantum mechanics the probability of electronic transitions decays exponentially with increasing distance. Evidently this means that a full analysis requires the neutralization process to be followed through the entire trajectory. Note that if an electron can hop from the surface to the atom, it may also be possible for the electron to hop back to the surface. The probabilities for these two processes are not necessarily the same. Hence, the ion maybe engaged in both neutralization and ionization processes during its scattering trajectory. In addition, each part of the trajectory will also have a different effect on the final charge state of the ion. This has been investigated by Aono [49,50] for various helium ion–atom combinations. The charge fraction of the detected particles is a reflection of the average charge state of the ions during the interaction.

Returning to figure 2.15a the first mechanism illustrated is Auger neutralization. This is a two electron process resulting in a ground state neutral atom. For this to proceed the incoming ion must have an unoccupied energy level of sufficient depth for the neutralizing electron. An electron from the solid first tunnels into a hole state on the ion and the excess energy is then used to liberate an electron from the conduction band. As in the case of Auger Electron Spectroscopy the energy of the Auger electron released depends on which levels are involved. A theoretical study of this process has been carried out by Cobas and Lamb and Hagstrum [45,46]. In figure 2.15b the one–electron process of resonant neutralization/ionization is depicted, in which an electron tunnels through the surface potential barrier into an available ion level of approximately the same energy, leading to a process which is non-radiative. If the ion's energy level is situated below the Fermi level of the metal, the reverse process of resonant ionization is unlikely. However, if the ion's energy level is broadened by reaction with the surface so that it straddles the Fermi level, resonant tunnelling can occur in both directions. An added complication is that the

energy levels of the ion shift as it approaches the surface, due to the image charge potential. As the ion approaches the surface the energy level decreases in negative potential energy and broadens [45,46]. In figure 2.15c the process Auger de–excitation depicted is a variation on 2.15a, though this time involves an excited atom rather than an ion. As before an electron from the solid tunnels into a deep ion energy level, but in this case the available excess energy is taken away by the electron situated in the excited energy state of the ion and the neutral atom is therefore de-excited. The emitted electron again carries information about the energy levels. In the final process (figure 2.15d) quasi–resonant charge exchange and depicts an electron tunnelling from a deeper lying level in the solid into a deep level of the incoming ion leaving it in the ground state. The reverse process of the electron tunnelling from the now neutralized ion into the valence band is likely and produces the oscillations in the elastic ion scattering intensity detected, for ion–atom combinations with the relevant energy levels [101].

Because they are experimentally separable the trajectory is usually considered in three sections; the incoming path phase, the collision and the returning path phase [48,52,53,54,55]. This has been investigated by Aono et al. [21] for He^+ scattering off a range of materials. Their analysis demonstrates that for He^+ the main neutralization path is via the Auger neutralization for materials with work functions greater than 4eV. Close to this energy there are two helium energy levels, 2^1s at 4.1 eV and the 2^3s at 4.7eV [45]; which can become involved in resonant neutralization and ionization. According to Souda the resonant ionization has a probability of one, thereby leaving the helium atom in an ionized state [22]. For noble gas ions the dominant process is usually considered to be the Auger process (except for materials for which the energy levels are well matched for quasi–resonant charge exchange) due to the availability of deep hole states on the ion and this accounts for their small charge fraction. For alkali ions, the ionized energy level is close to the Fermi level [50] and the only available process is the resonant charge exchange. This, according to current ideas, has a much higher probability of occurrence, but the charge fraction is much larger, because the

equilibrium state is not neutral.

2.3.4. Features of Ion Scattering Spectroscopy (ISS)

The proceeding sections have dealt with the individual facets of a scattering experiment. In this section the various aspects are drawn together with relevant examples. Before performing an ISS experiment there are several details to consider, such as which ion should be used. In studies of elemental composition the important aspects are the surface sensitivity and specificity. These are linked to the neutralization probability, scattering cross-sections and shadow cone widths, which are all related to the depth of ion penetration. The significance of neutralization can be appreciated by considering figure 2.16, which depicts energy distribution spectra for He^+ and Li^+ ion scattering off Cu(110). The first thing to notice is the difference in the background. The Li^+ spectrum has a large inelastic background on which elastic peaks must sit, whereas the helium spectra is entirely devoid of an inelastic background. To the right of each spectrum is the copper binary collision peak. The backscattered flux is a mixture of scattering events from several layers. For helium ions the probability of neutralization for surface scattering is approximately 0.95, but this is greatly increased for ions penetrating below the surface which then have a very high probability of being neutralized [99]. Since the experiments usually detect ions the neutrals are ignored, hence the detected flux is only sensitive to the surface. In view of the fact that inelastically scattered ions, which could lead to a background, must penetrate below the surface to undergo such inelastic collisions, the ion background is low because these are precisely the trajectories most likely to be neutralized. The result is that there is no background below the elastic scattering peak in the energy distribution spectrum. This poses the question, why does lithium have a background and helium not? The answer lies in the difference in the neutralization mechanisms. Since we are detecting ions only in the experiment, the ion has to travel to the atom, undergo a collision and then return to the analyser in an ionized form. In lithium the ionized state is much shallower than for helium. This has the effect of shifting the charge equilibrium more in favour of the ionized state [71]. Consequently, the scattered ions

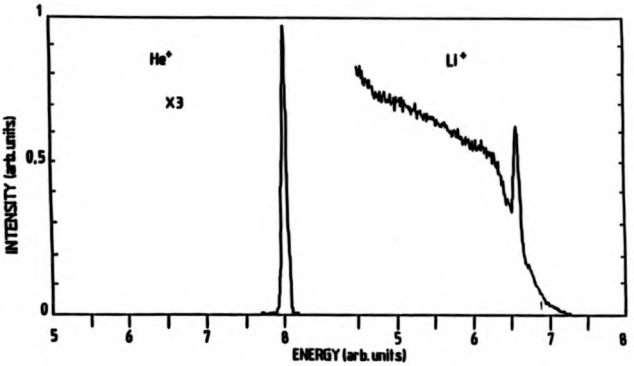

Figure 2.16 A comparison of the energy distributions for 1 keV helium ions and 3 keV lithium ions, indicating the differences in the inelastic background.

will return with a wider range of energies and this will manifest itself as a background.

In the discussion presented, the scattering has been dealt with in terms of a single collision, though the ion does not have to only scatter off a single atom. However, multiple collision trajectories can be treated as a series of binary collisions. This then allows the determination of the final energy of the ion for a given number of collisions. I.Terzic [100] produced a formula for n scattering events of equal scattering angle collisions, which has the form:–

$$\frac{E_1}{E_o} = \frac{1}{(1+A)^{2n}} \cdot \{ \cos^2\theta + (A^2 - \sin^2\theta)^{1/2} \}^{2n} \qquad (14)$$

If this equation is applied to a two event scattering trajectory, it is discovered that the final ion energy is larger than for the single atom scattering collision. This leads to the possibility of additional peaks in the energy distribution spectrum due to multiple scattering events. Thus the ions may return to the detector via a variety of scattering events, though for He^+ ion scattering the more tortuous trajectories will have associated enlarged neutralization probabilities.

When studying the intensities of the energy distribution scattering peaks the question arises; how is the elemental concentration related to this? The first problem is the effect of the neutralization which will vary depending on the ion used and the element under investigation. In addition to this, the intensity is dependent on the scattering cross-section of the atom. Classically this is defined as [42,84,86].

$$\frac{d\sigma(\theta)}{d\Omega} \cdot d\Omega \cdot N_S = \frac{\text{nos of particles scattered into solid angle } d\Omega \text{ /unit time}}{\text{Incident intensity}} \qquad (15)$$

where

$\sigma(\theta)$ = the differential cross–section

N_S= the number of scatters

By considering a general scattering process, see figure 2.17, the differential cross-section can be determined [84,86]:-

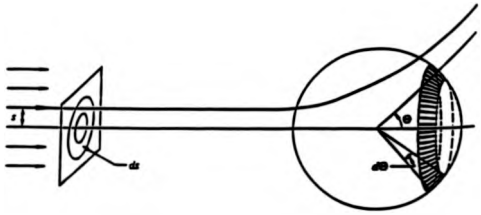

Figure 2.17 A general scattering process for a particle with an impact parameter of S and scattering into a scattering angle of Θ. (H.Goldberg, Classical Mechanics 2nd Ed. Addison-Wesley Pub. Comp. (1980))

$$\sigma(\theta) = \frac{S}{\text{SIN}\,\theta} \cdot \frac{dS}{d\theta} \qquad (16)$$

where

S = the impact parameter

For this to be determined theoretically the form of the potential needs to be known. Accurate calculations are most reliable for high energy ion scattering where the Coulomb potential is applicable. Alternatively, one can attempt to perform calibration experiments. For noble gas ions this may not always be possible due to non-linearities in the scattering intensity versus concentration curve [90]. For a calibration to be valid the neutralization rate must be constant, but it is known that the neutralization depends upon the surface electronic structure. If the surface reconstructs the neutralization rate may change [90] and in addition adsorbates leading to large work function changes are likely to lead to major changes in neutralization rates.

2.4. References

1. W. Heiland, F.Iberl, E.Taglauer and D.Menzel, Surface Science **53** (1975) 383
2. C.J. Barnes, M.Lindroos, D.J.Holmes and D.A.King, Surface Science **219** (1989) 143
3. D.L. Adams, H.B. Nielsen and J.N. Andersen, Surface Science **128** (1983) 294
4. G.P. Thompson and A. Reid, Nature **119** (1927) 890
5. C.J. Davisson and L.H. Germer, Nature **119** (1927) 558
6. J.B. Pendry, Low Energy Electron Diffraction. Academic Press (1974)
7. M.A.Van Hove, W.H.Weinberg and C.M. Chan, Low Energy Electron Diffraction. Springer - Verlag Berlin Heidelberg (1986)
8. L.J. Clarke, Surface Crystallography. John Wiley and Sons (1985)
9. G.A. Somorjai, Principles of Surface Chemistry. Prentice-Hall Inc. (1972)
10. M. Prutton, Surface Science. Clarendon Press (1983)
11. D. McKie and C. McKie, Essentials of Crystallography. Blackwell Scientific Publications (1986)
12. J.H. Onerferko and D.P. Woodruff, Surface Science **91** (1980) 400
13. P.Auger, J. Phys. Radium **6** (1925) 205
14. P.W. Palmberg, G.E. Riach, P.E. Weber and N.C. MacDonald, Handbook of Auger Electron Spectroscopy. Physical Electronics Industries Inc. (1972)
15. D.P. Woodruff and T.A. Delchar, Modern Techniques of Surface Science. Cambridge University Pree (1986)
16. J.Alvarez and M.C. Asensio, In Methods of Surface Analysis, PartA. Ed. J.L. Fierro. Elsevier Amsterdam (1989)
17. L. Harris, J. Appl. Phys. **39** (1968) 1419
18. N.J. Taylor, Rev. Sci. Instrum. **40** (1969) 792
19. L.Gonzalez, R. Miranda, M. Salmeron, J.A. Vaergas and F. Yndurain, Phys. Rev. B. **24** (1981) 3245
20. H.Siegbahn and L. Karlsson, Photoelectron Spectroscopy Handbuch D. Physik **31** Ed. W. Mehlhorn
21. M. Aono and R. Souda, Surface Science **179** (1987) 199

22. M. Aono, Nucl. Instr. and Meths. **B2** (1984) 374
23. O.B. Firsov, JETP **5** (1957) 1192
24. O.B. Firsov, JETP **6** (1958) 534
25. A.A. Abrahamson, Phys. Rev. **130** (1963) 693
26. O.S. Oen, Surface Science Letts. **131** (1983) L1407
27. C.S. Chang, U. Knipang and I.S.T. Tsong, Phys. Rev. **B28** (1987) 493
28. C.S. Chang, U. Knipang and I.S.T.Tsong, Nucl. Instr. & Meths. **B18** (1986) 11
29. A. Dygo & A. Turos, Nucl. Instr. & Meths. **B18** 115 (1987)
30. K. Mann, V. Celli and J.P. Tolennies, Surface Science **185** (1987) 269
31. Th. Fauster, Vacuum **38** (1988) 129
32. M.T. Robinson & I.M.Torrens, Phys. Rev. **B9** (1974) 5008
33. J.B. Gibson, A.N. Goland, M.L. Gram and G.H. Vineyard, Phys. Rev. **120** (1960) 1229
34. A.A. Abrahamson et al. Phys. Rev **121** (1961) 159
35. E. Taglauer & W. Heiland, Surface Science **33** 27 (1972)
36. W.L. Gay & D.E. Harrison, Phys. Rev. **135** (1964) A1780
37. M.T. Robinson & O.S. Oens, Phys. Rev. **132** (1963) 2385
38. I.M. Torrens, Interatomic Potentials (1972)
39. H.Massey, Atomic & Molecular Collisions
40. C.Kittel, Introduction to Solid State Physics
41. R.E. Johnson, Introduction to Atomic & Molecular Collisions
42. L.C. Feldman & J.W. Mayer, Fundamentals of Surface & Thin Film Analysis
43. D.P. Woodruff & T.A. Delchar, Modern Techniques of Surface Science
44. E.Langley, Phys. Rev. **111** (1958) 91
45. A. Cobas & W.E. Lamb, Phys. Rev. **65** (1944) 327
46. H.D. Hagstrum, Phys. Rev. **96** (1954) 336
47. E.S. Parilis & L.M. Kishinevshii, Sov. Phys. Solid State **3** (1960) 885
48. R. Souda and M. Aono, Nucl. Instr. & Meths. **B15** (1986) 138
49. R. Souda, M.Aono, C. Oshima, S. Otani and Y. Ishizawa, Surface Science **150** (1985) L59
50. R. Souda & M. Aono, Nucl. Instr. & Meths. **B15** (1986) 114

51. R.J. Carbone, E.N. Fuls and E. Everhart, Phys Rev. **102** (1956) 1524

52. R.J. Macdonald, D. O'Connor and P. Higginbottom, Nucl. Instr. & Meths. **B2** (1984) 418

53. R.F.Garret, R.J.MacDonald & D.J.O'Connor, Surface Science **138** (1984) 432

54. R.F.Garret, R.J.MacDonald & D.J.O'Connor, Nucl. Instr. & Meths. **218** (1983) 333

55. D.P. Woodruff, Surface Science **116** (1982) L219

56. R.J. Macdonald and P.J. Martin, Surface Science **111** (1981) L739

57. R. Souda, T. Aizawa, C. Oshima, S. Otani and Y. Ishizawa, Surface Science **194** (1988) L119

58. D.J Godfrey & D.P. Woodruff, Surface Science **105** (1981) 438

59. G.G. Ross, Nucl. Instr. & Meths. **B15** (1986) 146

60. J.A. Yarmoff & R.S. Williams, Surface Science **166** (1986) 10

61. G. Engelmenn, E.Taglauer and D.P. Jackson, Nucl. Instr. & Meths. **B26** (1987) 522

62. G.E. Chapman, D.J.O'Connor and R.J. MacDonald, Nucl. Instr. & Meths. **B21** (1987) 20

63. W. Eckstein, Molchanov & H. Verbeek, Nucl. Instr. & Meths. **149** (1978) 599

64. K.J. Snowdon, R. Hentschke, A Narman, W. Heiland, E. Mühling and W. Eckstein, Nucl. Instr. & Meths. **B23** (1987) 309

65. F.W. Meyer, C.C. Hanvener, S.H. Overbury, K.J. Snowdon, D.M. Zehner, W. Heiland and H. Hemme, Nucl. Instr. & Meths. **B23** (1987) 234

66. A. Niehaus, Nucl. Instr. & Meths. **B31** (1988) 359

67. H. Lee & T.F. George, Surface Science **172** (1986) 211

68. K.W. Sulston, A.T. Amos and S.G. Davison, Surface Science **197** (1988) 555

69. M. Tsukada, S. Tsuneyuki & S.G. Davison, Surface Science **164** (1985) L811

70. J. Hermann, J. Gehring and V. Kempter, Surface Science **171** (1986) 377

71. S.H. Overbury, Nucl. Instr. & Meths. **B2** (1984) 384

72. A. Modinos & S.I. Easa, Surface Science **185** (1987) 569

73. A. Ishii, Surface Science **192** (1987) 172

74. W.F.Engelhoff, Surface Science Repts. **253** (1987)

75. P.Varga, App. Phys. A. **44** (1987) 31

76. J.J.Gerling, L.F. Tz. Kwakman and J.Los, Surface Science **184** (1989) 305

77. A.Narmann, H. Derks, W. Heiland, R. Monreal, E. Goldberg and F. Flores, Surface Science **217** (1989) 255

78. T.M.Buck, Y-S Chen, G.H. Wheatley and W.F. Van Der Weg, Surface Science **47** (1975) 244

79. M.Gryzinski, Phys. Rev. **138** (1965) 14336

80. A.G.J. DeWit, G. A. Van Der Schootbrugge and J.M.Fluit, Surface Science **47** (1975) 258

81. R.P.N. Bronkers and A.G.J. DeWit, Surface Science **104** (1981) 384

82. V.V. Afrosimov & N.V. Fedorenko, JETP (1958)

83. N.V. Fedorenko, Sov. Phys. Uspeki **2** (1959) 526

84. H.Goldberg, Classical Mechanics 2nd Ed. Addison-Wesley Pub. Comp. (1980)

85. S.Rubin, Nucl. Instr. and Meths. **5** (1959) 177

86. E. Taglauer and W. Heiland, App. Phys. **9** (1976) 261

87. D.P. Smith, J. Appl. Phys. **38** (1967) 340

88. P. Sigmund, Phys. Rev. **184** (1967) 340

89. D.P. Smith, Surface Science **25** (1971) 171

90. H. Niehus and E. Bauer, Surface Science **47** (1975) 222

91. B.V. Pannin, JETP **15** (1962) 215

92. S. Datz and C. Snoek, Phys. Rev. **134** (1964) A347

93. H. Hulkpe, Surface Science **52** (1975) 615

94. V.V. Afroeomov, Sov. Phys-Tech Phys. **2** (1957) 2391

95. J.W.Rabalais, T.R.Schuler & O.Grizzi, Nucl. Instr. & Meths. **B28** (1987) 185

96. W. Eckstein, Nucl. Instr. and Meths. **B27** (1987) 78

97. A.A. Abrahamson, Phys. Rev. **178** (1969) 76

98. Yu. V. Martynenko, Rad. Effects **20** (1970) 211

99. H.H. Brongersma and T.M. Buck, Nucl. Instr. and Meths. **149** (1978) 569

100. I. Terzic, D. Ćirić and B. Pervic', Surface Science **85** (1979) 149

101 R.L.Erickson and D.P.Smith, Phys. Rev. Letters **34** (1975) 297

Chapter 3.
Apparatus

3.1. The Chamber

The apparatus consists of a two level stainless steel ultra high vacuum (UHV) chamber with a base pressure of approximately 10^{-10} mbar. A schematic of the chamber is presented in figure 3.1. On the upper level is situated a forward viewing V.G. Scientific LEED optics used for checking the surface ordering. Alongside this are the resistively heated alkali metal SAES getter sources, which provide impurity–free alkali dosing of the sample surface used in some of the experiments reported here. The main detection system utilized in the ion scattering experiments is situated on the lower level and consists of a VSW HA50 concentric hemispherical analyser. Situated next to it is the ion gun used for the Low Energy Ion Scattering (LEIS) measurements, and in order to perform Auger electron spectroscopy an electron gun is situated alongside the ion gun. Sample cleaning was performed by Argon ion bombardment using a VG Scientific AG2 ion gun situated between the two levels. Argon and the gases used for adsorption studies were leaked into the chamber via leak valves from a gas manifold. To maintain UHV conditions the chamber is pumped by a liquid nitrogen trapped oil diffusion pump, an ion pump and a titanium sublimation pump and in addition the LEIS ion gun is differentially pumped by a turbo molecular pump when operating with a gas source.

3.2. The Manipulator

The sample manipulator was designed and built in the Surface Science group at the University of Warwick. For Impact collision Ion Scattering Spectroscopy (ICISS) measurements the accuracy of the manipulator is crucial, since all inferences concerning the surface structures ultimately depend upon it. The main considerations

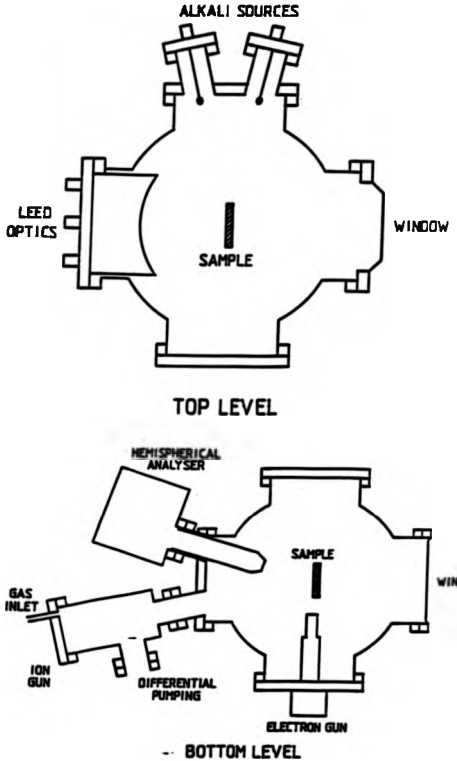

Figure 3.1 A schematic of the equipment arrangement on the two level UHV stainless chamber used in the project.

for the manipulator were:-

1. Accurate and repeatable polar rotation about the manipulators central axis
2. Repeatable azimuthal rotation around an axis perpendicular to the sample face.
3. Accurate and repeatable positioning of the sample laterally and vertically.
4. Electrical and thermal isolation of the sample.
5. Efficient sample cooling and heating.
6. Minimization of size due to the lack of available space.

The final design of the sample stage is shown in figure 3.2. For ICISS the first two points are the most important. Repeatability in azimuthal rotation was obtained by the use of gearing to provide a direct drive to the sample. This also minimized the effects of rotational backlash and through the use of gear reduction an accuracy of approximately 1/3rd a degree was obtained. In practise the azimuthal accuracy was limited by the use of LEED to orientate the crystal to the desired azimuth.

The sample stage was mounted on a hollow tube which was able to be rotated about its axis along its length and thereby provide polar rotation. This polar rotation was facilitated by mounting the support tube on a differentially pumped Vacuum Generators rotary seal. This arrangement entirely decoupled the polar and the azimuthal angles. The support tube also formed a liquid nitrogen dewar to enable the sample to be cooled. Before any data were taken the zero positions and the accuracy of the rotation had to be determined. When the crystal is rotated there are two sources of uncertainty, one is the accuracy of the polar rotation about the central axis and the other comes from the tilting ('wobbling') of the sample as it is rotated azimuthally. The former was solved by accurate machining about the center of rotation using a lathe and then checked again by measuring the displacement of the sample before and after mounting it in the vacuum chamber as a function of the polar angle. To measure the tilt of the sample, laser reflection was used. In this method the displacement of a laser beam is measured after it has reflected off the sample for different azimuthal angles. These values were then used to correct the angles of incidence in the ion scattering spectra (±1°).

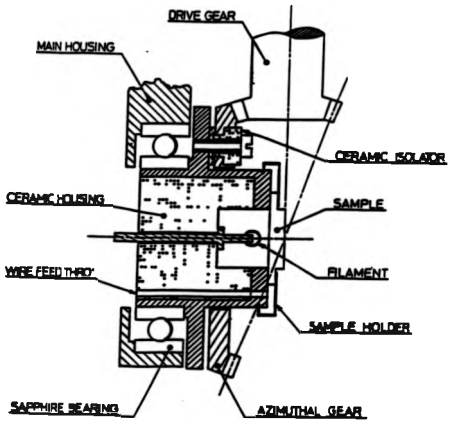

Figure 3.2 A cross-section of the sample holder used for the ICISS experiments, which provided both azimuthal and polar rotation coupled with X,Y and Z translation of the sample.

The lateral motion of the sample was obtained by utilization of two micrometer drives positioned perpendicular to each other. To obtain vertical motion a two stage system was used consisting of a three position compressed air driven system and a precision rotary thimble. The compressed air system was used to move quickly to identical positions on the various levels and the precision drive then allowed positioning of the sample over a 25mm vertical distance. Efficient electrical and thermal isolation coupled with a reasonable cooling rate were obtained by using sapphire ball bearings in the gearing and using the main support block as a cooling path, which allowed a cooling braid to be omitted, thereby reducing the torque on the azimuthal motion of the sample. These design features produced a manipulator capable of independent accurate and repeatable azimuthal (±1/3°) and polar rotation (±1/2°) about the sample center.

3.3. Analyser and Ion Gun

The complete ion gun and analyser assembly was manufactured by VSW Instruments and mounted on a 200mm flange and consists of a multichannel HA50 concentric hemispherical analyser and a mass filtered ion gun. They are mounted so that the total scattering angle is 150°, see figure 3.3. The ion gun is capable of producing an ion beam from two different sources, either a gaseous source subject to electron bombardment to form the ions, or a solid resistively heated source with a maximum kinetic energy of 3 keV. In this project the former was helium and the latter was a lithium source obtained from Spectramat Inc. The exchange of gaseous sources only requires the changing of a gas bottle, but the changing of the solid source requires the whole ion gun to be dismantled. The ions produced are then mass filtered by the use of a quadrupole mass spectrometer floated to a voltage corresponding to the required kinetic energy. The ions then pass through a focussing system and onto the sample. In order to increase the gas pressure in the ionization region for a gaseous source the ion gun was differentially pumped, thereby increasing the ion current.

The ion gun has three different modes of operation, they are referred to as:– 1.

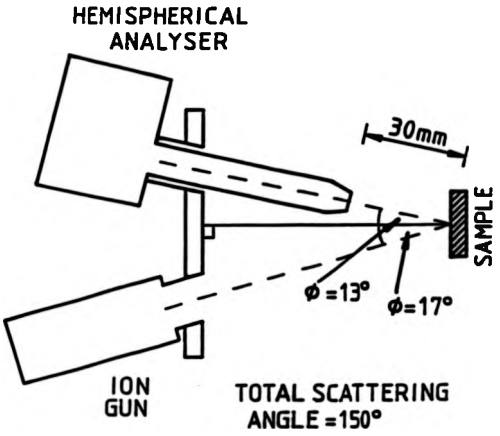

Figure 3.3 The positioning of the concentric hemispherical analyser and ion gun relative to each other and the sample under investigation.

"Emission", 2. "Current" , 3. "Beam". The first mode maintains a constant value for the electron emission current and was used for the gaseous sources. In the current mode the current applied to the solid ion source is maintained at a constant value. The final mode was used in the ICISS studies and produces a constant beam current. This is achieved by measuring the ion flux impinging on a high transmission grid at the exit aperture of the ion gun and then controlling the filament current to maintain this flux at a constant value. The positioning of the grids ensures that only the constituents of the ion beam which are used to scatter off the sample are measured. The variation in energy of the ion beam was found to be ±1 eV, obtained by monitoring its energy using a high accuracy digital voltmeter.

The analyser is a HA50 modified to perform multichannel detection in order to enable higher rates of data acquisition. The detected ion flux is focussed by electrostatic lenses onto the entrance aperture of the hemispheres, figure 3.4. Only ions that have energies within a defined energy window are then transmitted, and are linearly dispersed across the exit apertures. To produce this linear dispersion the analyser is operated in a fixed analyser transmission mode (FAT) at a fixed pass energy. After leaving the exit aperture the ions strike a pair of microchannel plates which produce an electron pulse per ion. The electron pulse then strikes a position sensitive resistive encoder.

The resistive encoder has two connections, plus a pulse validation connection, which monitors the electric charge deposited on it. When an electron cloud strikes the position encoder the total charge divides up into two parts whose size ratio is dependent on their initial position on the encoder. The rise times of these pulses are detected by timing electronics from which the energy of the detected ions can be determined, due to the linear dispersion of energies upon the encoder. The multichannel characteristic is due to the analyser transmitting a range of energies to the channel plates. This window of accepted energies is then scanned across the desired energy range, thereby scanning each ion energy from one side of the encoder to the other and therefore compensating for any non linearities that exist in the

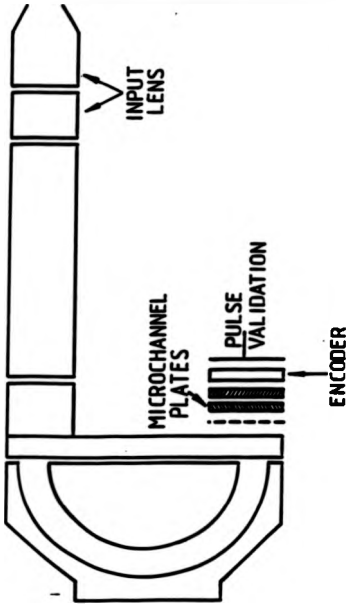

Figure 3.4 Outline of the multichannel detection system contained within the HA50 concentric hemispherical analyser.

microchannel plates and associated position sensitive dectector.

The electronic pulses from the detection electronics of the analyser are then fed to a multichannel analyser which updates an energy distribution display in real time. These spectra were then stored on a mainframe computer ready for analysis. The analyser offers a range of scanning speeds (0.1–1000 eV/s) and fixed energy windows to scan over, up to a maximum energy of 5keV. In addition the pass energy can be varied from 25–250 eV. The polarity of the analyser potentials can also be switched to permit the detection of electrons, thus providing the ability for Auger electron spectroscopy to be performed.

Chapter 4.
Application of Impact Collision Ion Scattering Spectroscopy (ICISS) for the Investigation of Cu(110)

4.1. Introduction

In LEIS, a scattered ion energy spectrum at a fixed scattering angle exhibits a number of binary collision peaks, from which the identity of the elements present on the surface can be deduced. In addition there is some structural information. A refinement of this technique which is particularly well suited to obtaining the structural information is to use a scattering angle as close to 180° as is possible, thereby reducing the scattering events to head on collisions. This is known as Impact Collision Ion Scattering Spectroscopy or ICISS. In the case of He^+, in particular, the structural information can be obscured by the effects of trajectory dependent neutralization, and one way to overcome this problem is to use alkali ions; the technique is then known as Alkali Impact Collision Ion Scattering Spectroscopy (ALCISS) [6,8,9,13,15,17]. It is this latter technique that is applied in the series of results presented. The ion beam consisted of Li^+ ions, which were energy and mass selected.

The Cu(110) surface has been studied extensively by several groups using a wide variety of techniques [6,8,10,14,20,23,24,26]. From these there has emerged a consensus concerning the value of the structural parameters. Namely, the first to second layer spacing is compressed by approximately 5% and the second to third layer spacing expanded by 2.5% compared to the bulk values [8,20,24,26]. This well characterized system was used to test our new apparatus and to differentiate between different methods of data collection.

4.2. Impact Collision Ion Scattering Spectroscopy (ICISS)

ICISS is a specialization of ion scattering, which is particularly aimed at the determination of structural parameters, such as inter–layer spacings. It was first developed in Japan by M.Aono and his coworkers [1,22] in the early eighties and has since been adopted by several groups. The basis of the technique is the concept of shadow cones, see section 2.3.2, and their interaction with the crystal. The only special requirement in the ion scattering equipment is in the near 180° scattering angle used. In ion scattering generally, a range of angles have been used, although a particularly convenient angle to use is 90°, for which the scattering equations simplify. For ICISS the scattering angle is chosen so as to be as near to 180° as is physically possible. A schematic of the scattering condition is presented in figure 4.1. When an ion undergoes a 180° scattering event its impact parameter is essentially zero. The structural determination relies on the finding of the relative positions of the atoms, which is achieved by using the enhanced flux intensity at the edge of shadow cones, see section 2.3.2. Consider figure 4.2, in which each atom is on the edge of its neighbour's shadow cone. In this situation, each atom is being subjected to an increased ion flux due to the focussing by the shadowing cones, and an increased scattering signal is seen. If the angle of incidence is altered, the shadow cones rotate about the shadowing atom, then each time the shadow cone intersects an atom an increased scattering signal results just at the threshold conditions at which a step occurs due to a new scattering event. If the scattered flux is plotted against the angle of incidence, several peaks superimposed on steps will be obtained corresponding to the shadowing thresholds of different atoms (for example see figure 4.3). From these peak positions the relative positions of the shadowed atoms to the target atom may be determined. Of course, in order to determine the relative position of the shadowed atom, the width of the shadow cone must be known. Experimental calibration of the shadow cone width can be achieved from the surface threshold conditions for known surface spacings if we note that the shadow cone width, figure 4.2, is given by:–

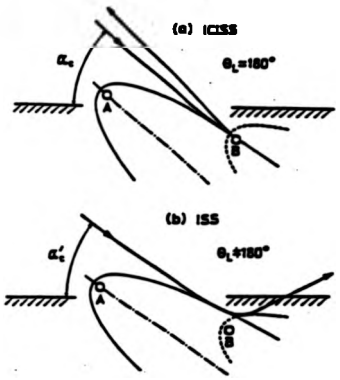

Figure 4.1 A comparison of ICISS (a scattering angle of =180°) with ordinary ISS (a scattering angle of << 180°). When the shadow cone of atom A crosses atom B in ICISS the ions scatter off the center of atom B allowing position determination, whereas in ISS this condition is not met. (M.Aono, Nucl. Inst. and Meths **B2** (1984) 374)

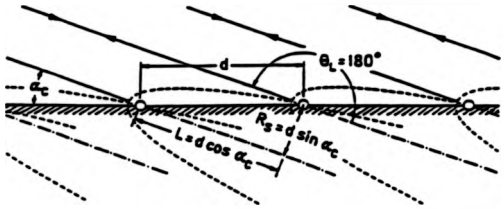

Figure 4.2 For the surface threshold condition each atom is emerging from its neighbours shadow cone with increasing angle of incidence. The shape of the shadow cone is determined by utilizing this condition in different azimuths, as illustrated. (M.Aono, Nucl. Inst. and Meths. **B2** (1984) 374)

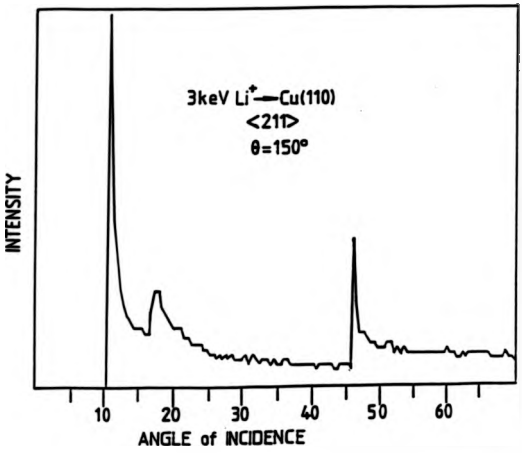

Figure 4.3 A computer simulation for 3keV 150° Li^+ ion scattering intensity variation as a function of the angle of incidence for the copper elastic peak intensity, from the clean Cu(110) with bulk parameters and no atomic vibrations. Note that the shadowing thresholds have very sharp leading edges.

$$R_s = d \sin \alpha_c \qquad (1)$$

where

d = The distance between the two atoms

R_s = The shadow cone width at distance d

α_c = The angle of incidence

To determine the relative position of the shadowed atoms from the peak positions in say figure 4.3, the width of the shadow cone needs to be known over a range of interatomic spacings. Absolute determination of the shadow cone width is not possible theoretically due to the ambiguity in the exact choice of the ion scattering potential. However, these shadow cone widths can be determined experimentally by utilizing the observed intensity peak angles for known threshold condition, using the bulk structural parameters derived from x-ray diffraction. Calibration of the shadow cone's width can therefore be performed on the clean surface using the position of the surface threshold conditions [4]. For this condition the detected signal will increase from essentially zero, thereby reducing any background effects. By determining the angular position of the surface enhanced edge for several azimuths, the width of the shadow cones can be determined at several distances behind the shadowing atom. In the ideal case the peaks in the angular distribution should have sharp edges, corresponding to the shadow cone's edge, figure 4.3. In reality these are usually less steep, i.e. softened, by thermal vibrations and instrumental effects, and it is necessary to define a criterion for locating the shadow cone threshold angular position. There have been several approaches to this condition such as taking the angle corresponding to the 50% or 70% position of the maximum peak height over the background [3,4,5,6,7,10]. It does not appear to have made an appreciable difference which condition is used, providing it is applied consistently, in calibrating and applying the shadow cones.

4.3. Data Acquisition

For the series of experiments performed a Cu(110) single crystal was used. This crystal was prepared using Laue X-ray alignment, spark machining and mechanical polishing to obtain the required crystal face. In UHV the crystal was subjected to Argon ion bombardment and annealing until LEED and LEIS indicated a clean and well ordered surface. It was found during this procedure that LEIS was a more sensitive probe of the structural quality of the order of the surface than LEED. The prominence of the surface enhanced edge in the angular spectra was very sensitive to the quality of the surface. Using this condition as an indicator the surface was argon ion bombarded and annealed in cycles until no further improved could be obtained. A large crystal (≈25mm) was used to minimize the effects of beam spillage off the edge of the crystal at very grazing angles of incidence. In the present experimental setup it is possible to collect the data in two possible modes, multiple channel and single channel. The data were initially taken in the multichannel mode to take advantage of the increased data acquisition rate. All previous studies had used single channel methods. To determine the cleanness of the sample a conventional LEIS spectrum was obtained using helium ions, usually having an energy of 1keV, and this proved particularly sensitive to the presence of low atomic number surface contaminants.

Our interest in this initial study was to investigate the change in the spectral line shapes of the ion–energy spectra with changes in the angle of incidence. One rather general feature of this type concerns the background in the LEIS spectra. It was discovered that Li^+ ion scattering was much less sensitive than the He^+ ion scattering to the presence of low atomic number adsorbates. The inability to detect adsorbates with lower atomic numbers than the substrate using Li^+ ion scattering is probably due to a combination of events. A general problem of large angle scattering is that the elastic scattering cross-sections are much smaller than at 90° as used in conventional LEIS, but an added problem is that the Li^+ ion spectra show a large inelastic background, figure 4.4. The signal to background ratio is small for low atomic number scatterers, making their scattering events difficult to observe in lithium ion scattering.

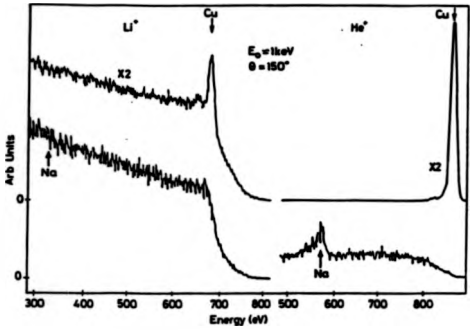

Figure 4.4 A comparison between Li^+ and He^+ 150° scattering from a clean Cu(110) surface and from the same surface after a large exposure to Na, illustrating the inability to detect Li^+ scattering from the Na adsorbates. The Li^+ spectra were collected with a primary energy of 1000eV and the He^+ spectra with a primary energy of 1080eV.

The lithium ions were therefore used mainly to study the substrate scattering features. Ion energy spectra near the substrate binary collision peak were monitored by placing an energy window around this region and recording the ion scattering intensities across it. This was repeated for each angle of incidence, which produced a series of energy distributions.

The analysis technique applied to the data depended on the method of collection. There are two stages to the analysis, the first is to extract the variations in the intensity of the monitored scattering peak in the energy distribution, and the second is the interpretation of the modulations; the latter will be dealt with in a later section. When only one energy corresponding to that of the binary collision peak is monitored (single channel mode), the modulations are obtained directly. In this case the detection energy needed to be constantly monitored to maintain its position at the center of the elastic scattering peak. Additionally the scattered intensity was recorded in an analogue mode. Using the multichannel mode, however, we have found that the substrate scattering spectral feature does not comprise a single peak, as may be seen in figure 4.5, which shows a series of energy spectra for Li^+ ions scattering off Cu(110). In each of the spectra there is a prominent binary collision peak, but also a higher energy peak and shoulder. If the spectra are analysed by determining the change in the maximum intensity (i.e. pseudo single channel detection, figure 4.6) one obtains a spectrum reminiscent of the usual ICISS spectra. A better method, however, might be to integrate the area under the elastic peak of interest, but one must then decide whether to include or exclude the background present in the Li^+ ion scattering spectra.

If the spectra in figure 4.5 are examined it can be seen that the background varies in intensity depending on the angle of incidence. Note that the spectra are not presented in strict ascending or descending order, but are arranged around the angular peaks of figure 4.6; thus the spectrum with the largest intensity is at the back, and corresponds to the condition associated with the center of an angular peak. The areas of the spectral peaks were numerically integrated using a linear approximation to the background. From this two dissimilar angular spectra were obtained, figures 4.7a &

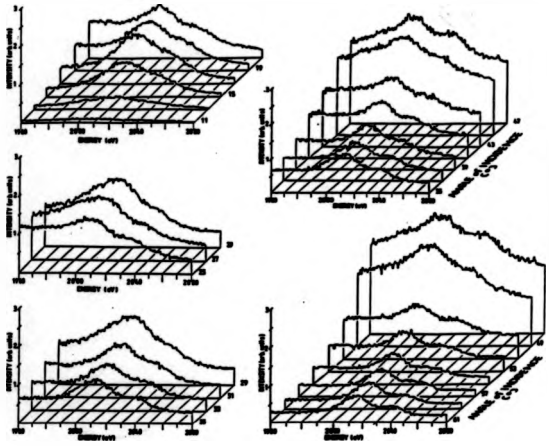

Figure 4.8 The 3keV Li^+ energy distribution curves located around the copper elastic peak for each angle of incidence from clean Cu(110) for a 150° scattering events. The energy distributions are not arranged in an ascending or descending order, they are arranged so that the maximum intensities seen in the pseudo single channel analysis, figure 4.6, are at the back of the plots.

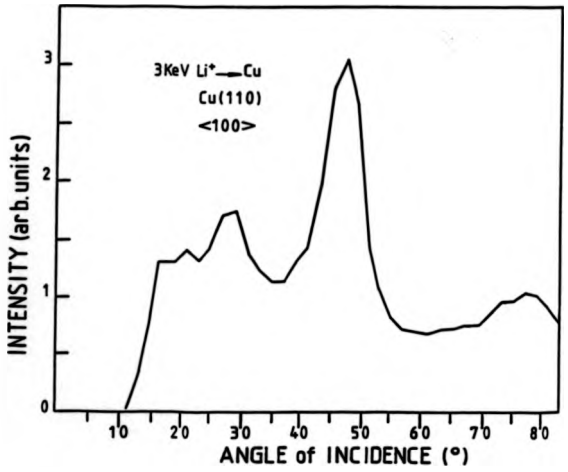

Figure 4.6 A pseudo single channel analysis of the 3keV Li^+ energy distributions for each angle of incidence scattering from a clean Cu(110) surface in the <100> azimuth. single channel analysis performed by taking the maximum intensity of the detected ions at the center of the copper elastic scattering peak.

4.7b, for integration with and without background subtraction. The integration without background subtraction, figure 4.7a, corresponds closely to the pseudo single channel result. However, when the background is subtracted the peak at the largest grazing angle of incidence disappears due to the background exhibiting an increase in intensity larger than that of the elastic peak itself. This is not the case for the two angular peaks with the shallowest grazing incidence angle. When the background is subtracted these peaks are enhanced. At these grazing angles the penetration of the incident ion flux is small, leading to a small contribution to the background and therefore the signal to background ratio is greater at these grazing angles of incidence.

In addition to the binary elastic scattering peak, there is another peak situated 20 eV higher in energy. This corresponds to a scattering event involving two atoms in which the collision angles are of approximately equal sizes (pseudo–double scattering). The detected scattered intensity to the right of these peaks is due to the multiply scattered ions.

In conclusion the variation in the peak intensity is complicated by a modulating background. This is not seen in heavier alkali metal ion scattering spectra due to their increased shadow cone widths, thereby reducing ion penetration into the crystal. Fortunately, the modulation of the combined background+peak intensities correlate with the changing shadowing conditions. Hence, to investigate the structure of the surface the total area underneath the elastic scattering peak must be monitored.

In view of this the final results were taken using a single channel analogue collection mode to increase the speed of data acquisition, since the multichannel scanning mode required more than three hours per angular spectra per azimuth. The main problem is not the contamination by the residual gases, but the surface degradation caused by ion sputtering. This required the incident ion current and the experimental time to be kept to a minimum. The alternative method utilized is experimentally equivalent to integrating within an energy window. In this case, the analyser energy window was set so that it was situated symmetrically about the binary

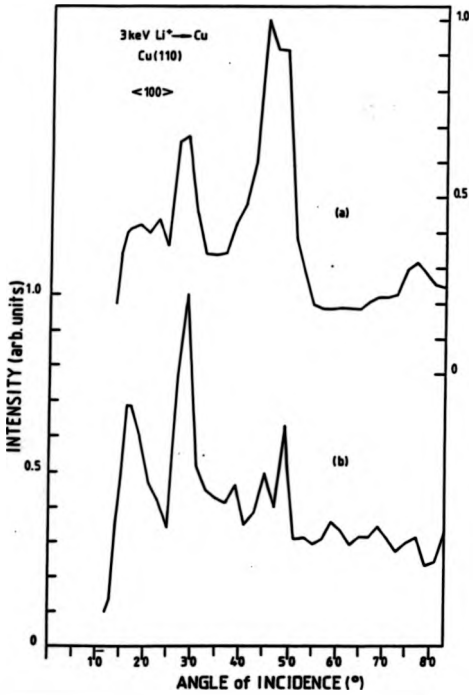

Figure 4.7 Two methods of obtaining the intensity modulation as a function of the angle of incidence when integrating the areas under the elastic copper peak, that is (**a**) without background subtraction and (**b**) with background subtraction. These spectra are for 3keV Li^+ ions scattering from a clean Cu(110) surface in the <100> azimuth for a scattering angle of 150° and are extracted from the data in figure 4.5.

collision peak, and then for each angle of incidence the detected ion flux was recorded directly. A reduction in experimental time was obtained since the analyser is now operated at a fixed energy. This allowed data for several azimuths to be taken for each surface structure preparation. All of the lithium scattering results were taken using this method. For weak scattering signals the original multichannel scanning mode was used. This usually occurred for low atomic number adsorbates for the scattering of helium ions.

4.4. Results and Data Analysis for Cu(110)

The results from the clean Cu(110) surface were obtained using 3 keV lithium ions, which gave better penetration to the second layer than could be obtained by using lower energies. 3 keV was the maximum energy at which our instrument could be used with safety, (for other energies see [2,8,9]). The angular scans were taken in the primary azimuths, <100>,<110>,<211> and <111>. These are presented in figure 4.8, and the azimuths used are defined for the clean Cu(110) surface in figure 4.9. All of the spectra have varying intensities and shapes which can be related to the surface structure. A first step towards this analysis was to use the observed surface threshold angles to determine the shadow cone shape for the Li ion/Cu atom combination, (see section 2.3.2). The position on the experimental edge used to define the critical angle, was chosen to be the angle corresponding to 70% of the threshold change in intensity [4].

Using this procedure the shadow cone width was determined at the surface threshold for each of the four principle azimuths, from which an experimental shadow cone was interpolated, see figure 4.10. This shadow cone was then used to predict the angular positions of the shadowing conditions for lower layer thresholds and to check whether these scattering events would be observed or whether they would be blocked. The determination of the angle of incidence for a shadowing condition is illustrated in figure 4.11a. In 4.11a atom 2 is shadowed by atom 1 and they are a distance d apart. Using the experimental shadow cone, the angle of incidence can be determined. By

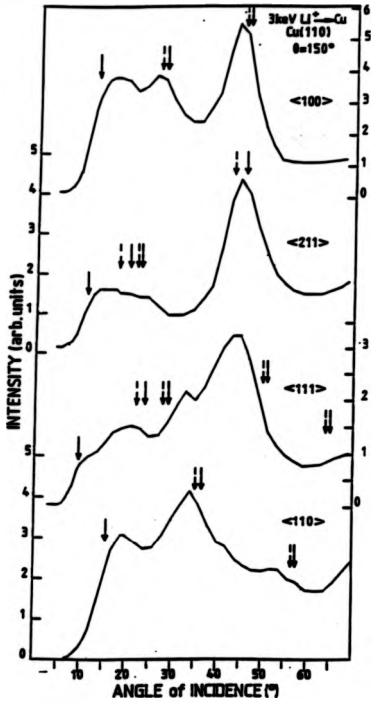

Figure 4.8 3keV 150° Li^+ ion scattering spectra for ions scattering from Cu atoms in a clean Cu(110) surface for the four primary azimuths. The variation of scattering intensity as a function of the angle of incidence spectra were obtained in a single channel regime. Simple shadow cone analysis predictions are shown by the arrows. For the bulk state the arrows have solid tails, and filled and unfilled heads indicate allowed and forbidden events respectively, arrows with dashed tails represent events events for a 1st to 2nd layer compression of 10%.

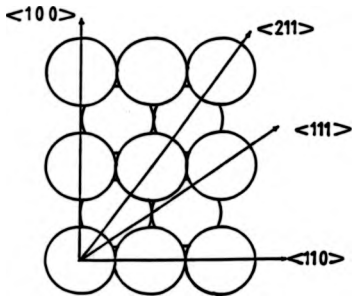

Figure 4.9 Definition of the four primary azimuths for a clean unreconstructed Cu(110) surface for which ion scattering data was obtained.

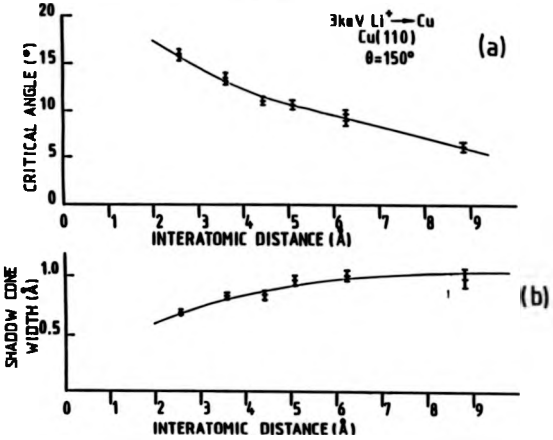

Figure 4.10 For each azimuth of the clean and oxygen dosed Cu(110) surfaces the position of the surface thresholds for 3keV Li^+ ion scattering was determined and plotted against the known atomic spacings (a). From this an experimental shadow cone was determined (b).

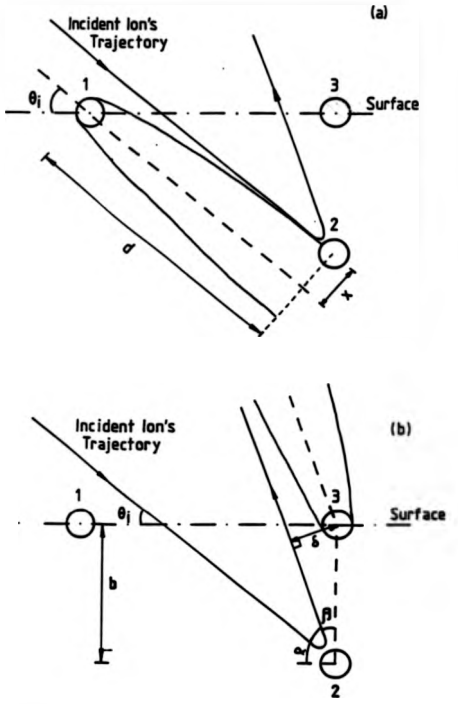

Figure 4.11 Using a knowledge of the interatomic distances between the shadower and the shadowed atoms coupled with a knowledge of the shadow cone's width, the angle of incidence at which the shadowing event occurs can be calculated (a). To detect this scattering event the ion needs to escape from the crystal and the possibility of this happening can be calculated (b).

adjusting the atomic parameters this can be made to fit the experimentally determined angular positions of the surface threshold. The possibility of blocking, (illustrated in figure 4.11b) must also be considered for each of the observed events. For example in figure 4.11b the ion trajectory can be blocked by atom 3. Using the theoretically determined angle of incidence and the known scattering angle (150° for these results) the distance of closest approach, d, to atom 3 can then be calculated. This distance is given by:

$$\delta = b \sin \beta$$

where $\beta = 90 - a$

$a = \theta_i - (180 - \theta_s)$

θ_s = Total scattering angle

b = layer spacing

θ_i = Angle of incidence

The distance of closest approach has to be compared to the maximum width of the shadow cone. If the shadow cone width is greater, the ion will be unable to reach the detector, i.e. the trajectory is blocked. An interesting problem is the definition of the maximum shadow cone width, because the scattering potential has an infinite range, so there is no exact solution to this question. In reality scattering by a very small angle is not a problem. For the present purpose, the maximum width was taken to correspond to the maximum measured value, which is adequate due to the inherent inaccuracy in the determinations of the shadow cone widths.

So far the involvement of a third atom in the scattering trajectory has only been considered as a potential source of blocking of the scattered ion. In actuality, it is also capable of modifying or displacing features (ref. [9] shows such an effect for Na^+ off Pt(110)). Note that the effect of atoms emerging from shadow cones leads to sharp rises in the signal with increasing grazing incident angles, whereas blocking leads to sharp drops in the signal with increasing grazing angles. In these cases the threshold

criteria (e.g. 70% peak height) must be necessarily on the trailing edge of the angular scan feature. A particular problem exists when shadowing and blocking conditions become close in angle, so that distinct edges cannot be separated effectively. In fact we find evidence that simple atom shadowing and blocking alone is not adequate to explain our data and that three atom scattering events appear to be important; this situation is depicted in figure 4.12. This figure depicts the variation of the scattering intensities for several types of shadowing and blocking events. In figure 4.12a the variation in the scattering intensity with incidence angle that atom b 'sees' due to atom a alone is depicted; this is a shadowing event and this signal would be the scattering intensity seen by the detector. Figure 4.12b illustrates the form of the scattering intensity for a blocking condition, note the intensity curve is reversed. A three atom scattering event is illustrated in figure 4.12c which incorporates both of the events in 4.12a and 4.12b. Graph 1 in figure 4.12c indicates the ion intensity that atom b sees due to a, and graph 2 depicts the intensity the detector would detect if atom b was a uniform source of ion flux by increasing the angle of incidence. From this combination of events, one, two or even no angular features may result. If peak 1 in graph 1 occurred well before the peak in graph 2 then two peaks would result. But if the two peaks coincide, or the angular spacing between them is less than or equal to the experimental resolution, only one peak will occur. No angular feature would occur if peak 2 occurs well after peak 1.

Using this approach the experimental angular spectra were analysed to try and account for lower layer scattering features. The results of this analysis are shown as arrows indicating where the predicted experimental features would occur for a bulk spacing and for a 10% compression of the first to second layer spacing, suggested by the data of [8,20,26] figure 4.8. It can be seen that only the <211> second layer feature coincides with these predictions. This feature is due to a straightforward shadowing event and suggests that the 1st to 2nd interlayer spacing is compressed by approximately 10% compared to the bulk value. A particular weakness of these simple theoretical considerations is that many of the experimental threshold features

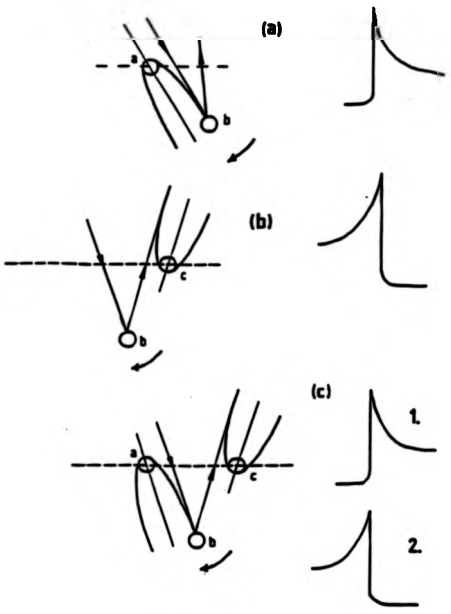

Figure 4.12 This depicts the changes in the scattering intensity for various scattering situations. The curved arrows indicate the direction of change of the angle of incidence measured relative to the sample. On the right are schematic plots of the intensity changes with increasingly less grazing angles of incidence. C represents a combination of the two previous situations, with graph 1 depicting the intensity that atom b sees, and graph 2 the ion intensity atom c would see if b was a uniform ion source.

correspond roughly to events predicted to be blocked (indicated by unfilled arrow heads), and suggests there is a breakdown of the simple model. The failure of this simple application of the shadow cone model occurs because many features are due to collisions involving more than two atoms. The importance of this type of collision appears to be due to the fact that the scattering angle used deviates substantially from 180° such that incident and scattered trajectories are far from colinear. In order to understand this problem, more sophisticated computer simulations allowing for multiple scattering effects were performed.

4.5. Description of Cu(110) Scattering Data by Computer Simulation

Several computer simulations of ion scattering from various surfaces have been published previously [8,11,12,21]. The program utilized in this project is aimed at predicting the structure of the angular scans, but no attempt is made to match exactly the intensities of the experimental spectra. The main reason for this is that the modelling is performed for a fixed periodic array and takes no account of thermal vibrations. Its main purpose is to predict features and to then enable understanding of the processes involved. This is possible since the computer generated trajectories can be followed.

The program follows a set of parallel in-plane trajectories for a particular angle of incidence individually through a series of collisions and determines their final trajectory and energy. Each of these trajectories is then compared to the assigned detector conditions, (angle and energy) and if it lies within these conditions the number of ions detected is incremented. This procedure is repeated over a range of angles of incidence; the number of sucessful trajectories for each incidence angle then form an intensity versus angle of incidence plot. This can be compared to the experimental data.

The program performs the simulation for a 2D array of scatterers representing a section perpendicular to the surface, to which all the coordinates are referenced. The

restriction to in-plane scattering events has not proved to be a serious constraint for the majority of scattering events, with the exception of the <111> azimuth to be discussed latter. The array can have two or three layers and is defined by inputting the periodicity and position relative to the top layer atoms (parallel to the top surface layer). The ions, with a defined energy and angle of incidence move with respect to this array in a straight line trajectory between scattering events. The calculations of the ion trajectory is determined by calculating the effect of one atom at a time. This atom is the one for which an apsis lies next along the current trajectory. The distance of closest approach and the resulting changes in momentum and energy are calculated with respect to this atom. After this calculation the ion is moved forward to a new apsis and has its direction changed by the appropriate scattering angle. This continues until the ion has left the influence of the crystal. Before an accurate simulation of an unknown system can proceed the scattering potential needs to be calibrated. This was performed by fitting theoretical calculations to the experimental data for the surface thresholds from the clean Cu(110) surface. The adjustable screening length scaling parameter in the Thomas–Fermi–Molière potential (see section 2.3.2) was tuned for the best agreement between the two predictions. It was found that reducing the screening length to 65% of its initial value, produced the best agreement.

After this the effect of a Cu(110) array on the detected scattering intensity was investigated. The results are compared with the experimental data in figure 4.13. Note there are no <111> theoretical data. This omission is due to the lack of out of plane scattering within the simulation. The need to consider out–of–plane scattering, in this particular azimuth can be understood by looking at the atomic structure along this azimuth, (figure 4.9). The spacing of the atomic planes perpendicular to this azimuth (≈0.43Å) is comparable with the width of the shadow cone so an in–plane scattering calculation is clearly inadequate. Calculations for the other azimuths reproduce all the main quantitative effects, but fail to reproduce the widths of the edges and peak. This is to be expected due to the use of a rigid lattice; inclusion of the effect of the thermal vibrations, which in reality reduce the focussing effect, requires the use of Monte

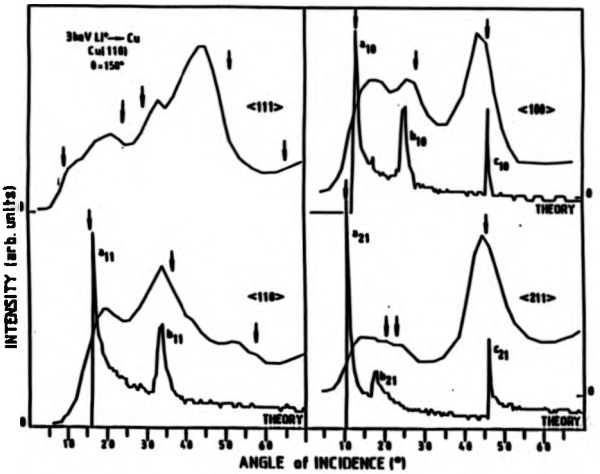

Figure 4.13 Theoretical scattering modulations as a function of the angle of incidence are compared with the 150° 3keV Li^+ ion scattering spectra for three of the primary azimuths.

Carlo methods leading to massive increases in computational time. This was felt to be inappropriate, since the aim was only to understand the events producing the experimental angular peaks. An example of the use of the Monte Carlo method can be seen in ref. 8, (Yarmoff et al.) for Li^+ scattering.

Figure 4.13 shows that the computer simulation reproduces all of the observed angular features. The trajectories leading to the observed experimental features are shown schematically in figure 4.14, which demonstrate that four of the discrepancies with the simple shadow cone model, peaks b_{10},c_{10},b_{11} and b_{21} were due to multiple scattering not included in these simple arguments. In the <110> azimuth the experimental peak b_{11} has a triangular shape, and the shape predicted by the simulation is similar to the b_{10} peak in the <100> azimuth. In both of these cases the ion has to thread its way between two layers, and its trajectory is altered by the top layer atom M in the <100> azimuth. If the positions of the shadow cones are considered along this path, (the simple shadowing model being useful once the trajectory is known), it can be seen that the volume of allowed trajectories through which the ion passes is small. The trajectory is constrained by shadow cones on two sides. The production of these angular peaks is a competition between blocking and shadowing trajectories, making the final determination of the peak shape far from easy. This is where the omission of atomic vibration becomes a problem, since a full calculation would help to determine which condition dominates. Where there is some uncertainty in the experimental data as to whether the peak is due to a shadowing or a blocking event, the theoretically determined trajectories have been used as the final arbiter.

Once the trajectories and their character have been determined the structural parameters can then be adjusted. The assignment of shadowing condition can be appreciated by comparing a_{10} and c_{10} peaks which are identical in form; this indicates that c_{10} must be a shadowing event. It is only possible to deduce information concerning the spacings of the top three layers from the data. In fact, only peak c_{21} contains information about the first to second layer spacing directly. All the other

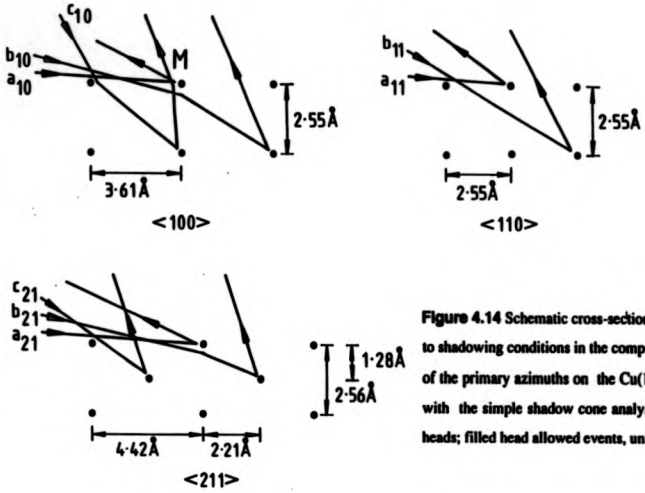

Figure 4.14 Schematic cross-section of the trajectories leading to shadowing conditions in the computer modelling for three of the primary azimuths on the Cu(110) surface. Comparison with the simple shadow cone analysis is shown by the arrow heads; filled head allowed events, unfilled heads forbidden events.

sublayer peaks can be attributed to first and third layer interactions, although a contribution from the second to the fourth layer must also be present. However, the calculations indicate that the first to third layer spacing is within a few percent of the bulk value. In contrast the first to second layer is compressed by approximately 10%.

One feature that is not fully explained by the modelling is the broad angular feature in the <211> azimuth extending from the surface threshold peak. The simulation predicts only two peaks, which might merge if thermal vibrations were included. These two peaks would appear not to account for the whole of the feature, and the reason for this broad peak is unclear.

4.6. Conclusions

In this section the limitations of using a simple shadow cone model have been investigated, and the results have been contrasted with those of a multiple scattering computer simulation. From this, it is concluded that the simple ICISS picture, *i.e.* a small impact parameter and one substantial collision only, is inadequate for a scattering angle of 150°. This angle is sufficiently far from 180° to require the use of computer simulations, due to the influence of multiple scattering events. This conclusion is at variance with that of Niehus [6] who used a 145° scattering angle and was apparently able to avoid the complications of multiple scattering. Niehus, however, used sodium ions for which the shadow cones are much wider. This limits penetration into the sample as well as shifting the thresholds to larger angles of incidence. These additional factors may be sufficient to block the multiple scattering events, though there is some evidence of an additional feature due to refocussing by the surface atoms in his data for $Na^+ \rightarrow Pt(110)$ [9]. The majority of the other 'ICISS' experiments performed by other groups have utilized scattering angles around 166°.

The simple shadowing model left many pieces of experimental evidence unexplained. In contrast, the computer simulation – though limited in only allowing in-plane scattering and failing to include thermal vibration – managed to provide an

explanation for all of the features of the experimental data and describe the scattering events involved. To understand peak shapes qualitatively the two models have been used together. The computer simulation identified the trajectories and the simpler shadowing model then allowed one to vizualize the effects by comparing the trajectory to the shadow cones of the surrounding atoms.

One key finding of the experiment is that changes in the background intensity are of key importance in measuring shadowing and focussing effects. This is important for lithium, but less important for heavier alkali ions which yield spectra with lower backgrounds. The results show that the makeup of the elastic peak is not necessarily simple.

When determining the shape of the shadow cones experimentally the surface threshold condition is utilized, a situation corresponding to the ion scattering off a chain of atoms. This is in marked contrast to substrate shadowing effects in which the shadow cone is used for scattering events involving only two scatterers. The computer simulations, however, were used to establish that there is negligible difference between the shadow cone widths produced in each case. Hence, it is valid to use the experimentally determined shadow cone to determine shadowing conditions. This suggests that the surface thresholds conditions are dominated by scattering from only a single shadower atom.

In addition to these points an estimation of the interlayer spacings has been determined for clean Cu(110) :-

1st to 2nd layer = (1.18 ± 0.03) Å

1st to 3rd layer = (2.61 ± 0.07) Å

2nd to 3rd layer = (1.43 ± 0.08) Å

Or in percentage terms compared to the bulk values

1st to 2nd layer = (8.0 ± 2.5) % compression

1st to 3rd layer = (2.5 ± 2.5) % expansion

2nd to 3rd layer = (12 ± 8.0) % expansion

The first to second layer spacing is in agreement with other groups [24,26] allowing for the large uncertainties. The value obtained for the second to third layer spacing, however, is rather large compared with the value found in several other studies of 2.5% expansion [24,25,26], but the error in our measurement is large. This large uncertainty in the second to third layer value is due to it being an interpolated value.

4.7. References

1. M. Aono, Jap. Journ. of App. Physics **V20** (1981) L829
2. M. Aono, R. Souda, Surface Science **179** (1987) 199
3. Th. Fauster & M.H. Metzner, Surface Science **166** (1986) 29
4. M. Aono, Nucl. Instr. & Meths. **B2** (1984) 374
5. H. Niehus, Surface Science **145** (1984) 374
6. H. Niehus & G. Comsa, Surface Science **140** (1984) 18
7. S.H. Overbury, Nucl. Instr. & Meths. **B27** (1987) 65
8. J.N. Yarmoff, D.M. Cyr, J.H. Huang, S. Kim & R.S. Williams, Phys. Rev. **B33** (1986) 385
9. H. Niehus & G. Comsa, Nucl. Instr. & Meths. **B15** (1986) 122
10. Th. Fauster, Vacuum **38** (1988) 129
11. A.D. Tenner, R.P. Saxon, K.T. Gillen, D.E. Harrison, T.C.M. Horn & A.W. Kleyn, Surface Science **172** (1986) 121
12. J.A. Yarmoff, R. Blumenthal & R.S. Williams, Surface Science **165** (1986) 1
13. H. Niehus & E. Preuss, Surface Science **119** (1982) 349
14. G. Engelmann & E. Taglauer, Surface Science **182** (1985) 921
15. M. Aono, R. Souda, C. Oshima & Y.Ishizawa Surface Science **168** (1986) 713
16. E. Taglauer & W.Heiland, Surface Science **33** (1972) 27
17. M. Aono, Nucl. Instr. & Meths. **B2** (1984) 374
18. H. Niehus, Nucl. Instr. & Meths. **218** (1983) 230
19. H. Niehus, Surface Science **130** (1983) 41
20. D.L. Adams, H.B. Nielsen & J.N. Andersen, Surface Science **128** (1983) 294
21. H. Derks, H. Hemme, W. Heiland & S.H. Overbury, Nucl.Instr. & Meths. **B23** (1987) 374
22. M. Aono, Phys. Rev. Letts. **V29** (1982) 567
23. R.P.N. Bronkers & A.G.J. De Wit, Surface Science **104** (1981) 384
24. I. Stensgaard, R. Feidenhans'l & J.E. Sorensen,Surface Science **128** (1980) 281
25. M.Copel, T. Gustafsson, W.R. Graham & S.M. Yalisove, Phys.Rev. B **V33** (1983) 453
26. H.L. Davis & J.R. Noonan, Surface Science **126** (1983) 245

Chapter 5.

Ion Scattering from Cu(110)(2x1)-O and Cu(110)(2x3)-N

5.1. Introduction

The Cu(110)(2x1)-O system has been extensively studied over the past fifteen years using a wide variety of techniques [1–12,15–21]. The structural variables of interest in this system are the exact position of the oxygen atoms and the nature of the surface reconstruction, (if any). A general concensus from previous studies places the oxygen atoms in the long bridge site in the <100> azimuth, figure 5.1. There is, however, a wide variation in the values proposed for the vertical displacement of the oxygen atoms, ranging from 0.6Å below the surface [1,2] to 0.3Å above the surface [3], with other values also being found within this range [4,8]. The values found from ion scattering experiments are mainly at the lower end of this range, and the upper limit is the result from a SEXAFS study. The reasons for this variation are unclear, although one reason maybe that the data were not obtained under identical surface conditions. In particular, some of the ion scattering experiments are performed under dynamical equilibrium conditions, whereby the crystal is in an atmosphere of oxygen throughout the experiment. This has been used to compensate for the sputtering of the surface by the ion beam [12]. Due to the erosion of the surface there is the possibility of new surface structures being formed [6,8]. In addition, a wide range of oxygen exposures from 10L [9], to 200L [12], all characterized by a (2x1) LEED pattern have been used. It is unknown whether the structure changes over this range of exposure, although it is known that a c(6x2) structure forms at very high exposures (10^6L [7]).

Several models have been suggested for the oxygen adsorbed surface structure. One structure is the missing row model [4,5,6,11,12] in which every second <100>

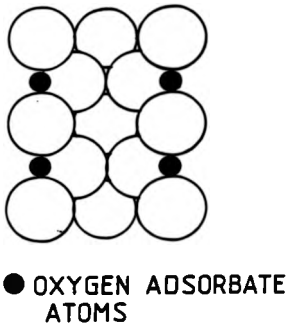

Figure 8.1 A missing row (2x1) reconstruction of the Cu(110) surface with the oxygen occupying the <100> long bridge site, in which every other <100> row is removed.

row is removed, figure 5.2. The removal of 50% of the surface atoms exposes the second layer, which may or may not be reconstructed. A small variation on this model is the saw-tooth model [4], also shown in figure 5.2. In this the missing row reconstruction is continued into the second layer, which then exposes the fourth layer. Further models are the shifted row, where every other <110> row is shifted vertically, and the paired row, where the <110> rows are shifted horizontally [1,11,20]. In the following section ICISS results for this surface are presented and discussed.

The final section of this chapter deals with a structure formed by nitrogen adsorption on the Cu(110) surface. The ion scattering data presented here provide clear evidence for a local reconstruction of the Cu(110) surface.

5.2.1. Cu(110)(2x1)-O Results

The oxygen reconstruction was formed by exposing a clean well ordered Cu(110) surface to a molecular oxygen atmosphere. The progress of the adsorption was monitored by LEED and was terminated when a good (2x1) LEED pattern was obtained. This procedure typically led to an oxygen dose of approximately 10L. Before acquiring the detailed lithium ICISS data the surface was examined using 1keV helium ion scattering.

The changes in lithium ion scattering intensity as a function of the angle of incidence for the oxygen dosed surface are presented in figure 5.3. Comparing these spectra to those obtained from the clean surface, it can be seen that the angular positions of the <211> and <110> surface thresholds have shifted to more grazing angles of incidence, whereas those in the <100> and <111> azimuths have not. These changes are consistent with a doubling of the atomic periodicity along <110>. In addition, most of the surface thresholds have become less distinct with one exception, that is the <100> azimuth. In this azimuth the surface peak has become more prominent. This is surprising since in this azimuth we anticipate oxygen shadowing of the surface if the oxygen resides above the surface in the long bridge site as previously

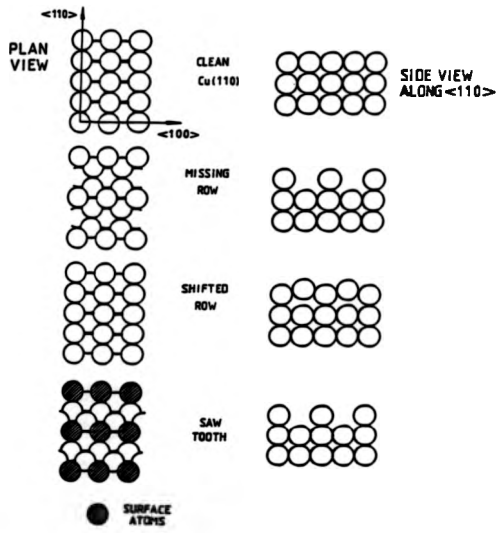

Figure 5.2 Comparison of various models for the (2x1) reconstruction for the Cu(110)(2x1)-O surface and their respective effects on the <110> azimuth.

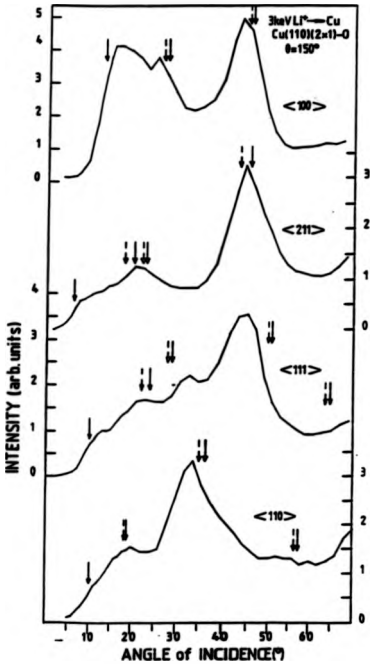

Figure 5.3 Ion scattering intensity modulation spectra as a function of the angle of incidence for 3 keV Li^+ ions undergoing a 150° scattering event from the copper atoms in the Cu(110)(2x1)-O surface for the primary azimuths. The arrows are the simple shadow cone analysis predictions for the missing row model, the complete tails are for the bulk interlayer spacings and the dashed for a compression of the 1st to 2nd layer compression of 10%. The unfilled and filled arrow heads indicate allowed and forbidden events.

proposed. Perhaps the most surprising feature of the data, however, is that there is very little change in any of the major peaks, both in their angular position and shape. This is particularly surprising because, as we have seen, the majority of these peaks are associated with multiple scattering within the top few layers of the clean surface, so if the surface is reconstructed we might expect these features to be sensitive to such changes. In particular, if the surface undergoes a missing row reconstruction, the main peak in the <110> azimuth at 36° should become a simple shadowing peak. One striking feature of the data, and especially the <100> azimuth surface threshold, is there does not appear to be any new shadowing due to the presence of oxygen.

In the <110> azimuth the peak at approximately 36° has become more prominent on the oxygen dosed surface, and has changed shape slightly, though these are exaggerated by the broadening and the attenuation of the surface threshold. The attenuation of this peak may be a result of a reduction of the number of scatterers, which would occur if the surface is reconstructed. Also, access to the second layer will be limited due to the oxygen atoms, which are expected to reside in the long bridge site, thereby reducing the scattering intensity further. These relative changes in intensities and shapes of features highlight the difficulty of interpretation of ion scattering angular scans. One other prominent change is that the broad angular feature above the surface threshold in the <211> azimuth has become narrower. This and other subtle changes will be discussed in the computer modelling section. The <111> azimuth, which cannot be modelled, exhibits some changes. For this azimuth a peak at an angle of incidence of approximately 21° for the clean surface, which was assigned to a second layer out of plane scattering event, has now become broader and less distinct; this may be a result of two slightly different scattering events being superimposed. One, of these is the first to second layer scattering event described above, and the other is the same event moved down one layer to become a 2nd to 3rd layer out of plane scattering event. For the clean surface spacings these scattering events would be separated by approximately 2°. These events are not seen simultaneously for the clean surface because the latter is blocked by the top-most

surface layer. If, however, the surface is reconstructed to a missing row type structure, then both events would be possible and would probably merge together to form a single feature.

Since lithium ion scattering is insensitive to low Z adsorbates [13] it is not the ideal tool for determining the position of the adsorbed oxygen atoms relative to the surface plane. Complementary helium ion scattering was therefore performed, in which a scattered signal from surface oxygen is obtained. Offset against this advantage, however, is the fact that helium ions suffer trajectory dependent neutralization [14] and also there is very little scattering from the lower layers. Trajectory dependent neutralization leads to enhanced neutralization at grazing angles and this limits the angular data range; we have concentrated on the region around the surface shadowing threshold condition. To aid the interpretation of the $He^+ \rightarrow O$ scattering signal, $He^+ \rightarrow Cu$ was also investigated. These angular scans for 2keV helium ion scattering are presented in figures 5.4 & 5.5 for the clean and oxygen dosed surfaces.

The $He^+ \rightarrow Cu$ scattering from both surfaces shows definite surface threshold edges, though those from the clean surface are a little sharper. This may be attributable to the enhanced neutralization in the presence of the oxygen adsorbate at these grazing angles of incidence. The results appear to be consistent with a (2x1) reconstruction of the surface, though the effects of neutralization prevent proper quantitative assessment of surface periodicity. The predicted surface thresholds for various vertical displacements of the oxygen atoms are marked on the figures based on the assumption that the oxygen atoms occupy the long bridge site. The expected positions for different substrate spacings are shown based on calculations using the same screening length correction as that utilized for the Li^+ scattering.

Turning to the $He^+ \rightarrow O$ spectra, it can be seen that the surface threshold features are much less pronounced than the $He^+ \rightarrow Cu$ ones. Calculated edge positions are shown, but take no account of neutralization which will tend to shift the edges towards

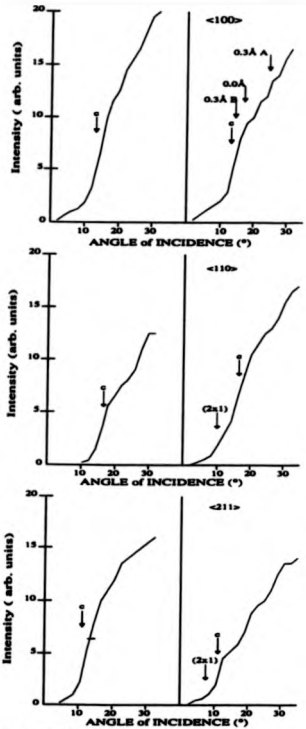

Figure 5.4 2keV 150° helium ion scattering intensity variations as a function of the angle of incidence from Cu in the Cu(110) and the Cu(110)(2x1)-O surfaces, left and right respectively. The arrows are the computer predicted thresholds, without neutralization, for various vertical displacements of the oxygen atoms in the <100> bridge site (A=above & B=below the surface) and for the missing row reconstruction.

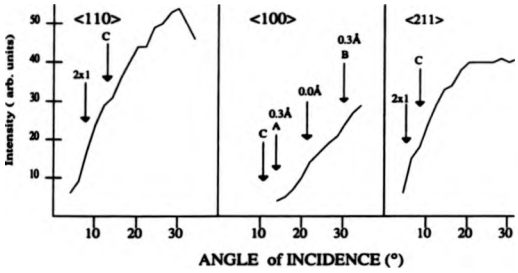

Figure 5.5 Ion scattering intensity modulation as a function of the angle of incidence for 2 keV 150° He^+ ion scattering from the oxygen atoms in the Cu(110)(2x1)-O. Where the letters A (above) and B(below) indicated the position of the oxygen atom relative to the top layer; C indicates the intensity thresholds for a (1x1) oxygen surface.

larger angles of incidence. These He^+ scattering data clearly rule out any subsurface oxygen model, since this would predict edges at larger angles of incidence than the experimentally obtained edges, i.e. they would predict an absence of signal, where a clear signal is seen. This suggests that the oxygen is either coplanar or above the top copper layer; a position of 0.3Å above the surface as suggested by SEXAFS [3] could be consistent with the data bearing in mind the uncertainty concerning the effects of neutralization. One further conspicuous feature of the $He^+ \rightarrow O$ signal is that the intensity seen in the <100> azimuth is substantially lower than in the other two azimuths, which are approximately equal. This suggests that the oxygen resides in the <100> long bridge site rather than in the four fold hollow site, which would tend to yield similar scattering intensities in all of the azimuths.

5.2.2. Modelling of Cu(110)(2x1)-O ICISS Data

In this analysis the aim was to use computer modelling of the ion scattering from model structures with the object of identifying the oxygen induced structure. Models considered are the missing row, saw tooth, shifted row and the paired row.

The missing row model, which is now widely regarded as the correct model, accounts for the doubling of the periodicity seen in LEED, and the doubling of the (110) row spacing seen in our data. With every other <100> row missing, the surface self-shadowing conditions will only be affected in the <110> and <211> azimuths, as can be seen in figure 5.2 depicting the MR reconstruction. Where the rows have been removed, the underlying layers have the same structure in the <100> direction as the clean unreconstructed surface, and therefore will give rise to features identical to those from the unreconstructed surface. These uncovered rows may mask the effect of oxygen shadowing in the <100> azimuth, which may be the reason why the experimental data exhibits no oxygen shadowing effects. We might also expect that the angular features that were composed of multiple scattering events from the clean surface would revert to simple shadowing events. This should cause changes in the angular peak positions by up to approximately 2°, but this is not observed.

Consider now figure 5.6 which depicts the <110> azimuth, and a first to third layer scattering event. For the unreconstructed surface this scattering event, c_{11} was blocked, whereas for the MR structure computer modelling suggests that it would be seen. In figure 5.7 the experimental data for the <110> and <211> azimuths, for which the atomic spacing doubles, are compared to compared predictions. The c_{11} event is predicted to occur at a scattering angle of approximately 58°, but the data of figure 5.7 show no feature at the predicted position. Although the simple modelling cannot be expected to predict the scattering intensity of any event reliably, note that this is a simple shadowing event, so it is difficult to understand why it should not be visible. The third layer d_{11} event is now also possible and there is some (weak) evidence of this in the experimental data. The computer modelling predicts that this should be a blocking type of feature, but in this angular range it is also expected to observe surface thresholds from the unreconstructed <110> rows which may conceal this effect.

In the <211> azimuth the missing row model leads to the prediction of a shadowing feature at an angle of incidence of 19°, which agrees with a feature in the experimental data. This agreement would seem to suggest that the 1st to 3rd layer spacing is equal to the bulk layer spacing, although this is at variance with other 1st to 3rd layer angular features which exhibit no change in angular position, and therefore indicate a 2.5% expansion. The above points would seem to mitigate against the missing row model. A model that is very similar to the MR model is the ST model in which the MR reconstruction is continued into the second layer. The differences between these two models would only be seen in the <211> azimuth. Calculations suggest that the ST model would require an extra feature at approximately 29° in this azimuth, which is not seen in the data. To reconcile this with the data would require a large expansion of the 2nd to 3rd layer spacing (≈30%), which would displace other features. This combined with the problems of the MR model would appear to rule out the ST model.

An alternative to atom row removal which also reproduces the doubling in spacing of atoms along <110> in the surface is to displace half of the atoms

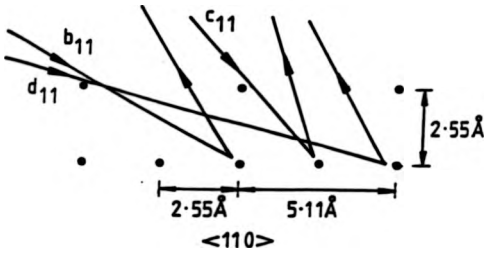

Figure 5.6 Previously forbidden trajectories that are now possible for 3keV 150° Li^+ ion scattering from copper atoms for a (2x1) missing row type reconstruction of the Cu(110) surface.

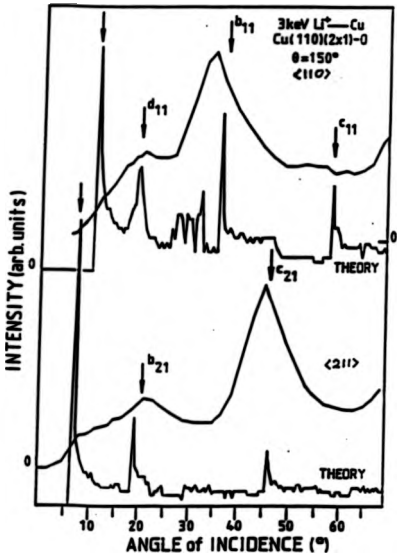

Figure 5.7 Comparison of the computer predicted ion scattering intensity modulation as a function of the angle of incidence, for 3keV 150° Li+ ions scattering from copper atoms for a (2x1) missing row type reconstruction in the <110> azimuth compared to the experimental data. Labels refer to the trajectories defined in figure 4.14.

perpendicular to the surface. This is the 'Shifted Row' model, also known as the 'Buckled row' or the 'Rumpled Row' model. Due to the rumpling there are now two distinct layers where there used to be one, each producing its own angular features. In addition, this displacement will affect the <110> and <111> azimuths, since they will have alternate rows of different lattice spacings. In order that these features agree with experimental data, the displacement will either have to be small enough to allow these two sets of features to merge, or to be such that the additional features are blocked and therefore excluded from the final spectra.

To determine the minimum size of the displacement, the surface thresholds were examined for several different displacement values. If the displacement is too small the surface thresholds are shifted back towards the unreconstructed values. From the modelling the minimum value was found to be 0.4Å , whereas the only experimental study supporting this model (using high energy He ions [1]) found a value of 0.2Å. The computer predictions are depicted in figure 5.8 for the <211> and the <110> azimuths. In the <110> azimuth the extra feature at 25° is due to shadowing between the shifted rows. To make this coincide with the experimental data the interlayer spacing or the displacement would have to be increased. To agree with experiment the feature would have to be shifted to approximately 31°. This would reduce the displacement and would therefore move the surface thresholds away from the experimental values. In addition the <211> azimuth has extra features predicted that can not be reconciled with the experimental data. These facts seem to exclude the Shifted Row model, along with the presence of the split peaks due to the top layers.

One other model, that was originally proposed to explain the 1x2 reconstructions seen on other metal surfaces, was the paired row model [20], in which the <100> rows move horizontally. Calculations reveal, as may be expected from simple shadowing arguments, that this model is unable to account for the large shift in the surface threshold (self-shadowing) edges (consistent with a doubling of the periodicity in the <110> azimuth).

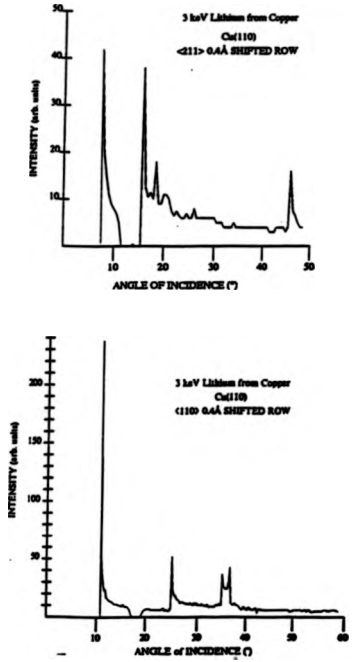

Figure 5.8 Computer predicted 3 keV 150° Li^+ ion scattering intensity modulations as a function of the angle of incidence from copper atoms with a 0.4Å relaxation of everyother copper atom perpendicular to the surface in the <110> azimuth for the <110> and <211> azimuths. Note the split peaks.

5.2.3. Conclusions for Cu(110)(2x1)–O

By using two complementary types of incident ions, information has been obtained concerning the position of the adsorbed oxygen atoms and the structure of the copper substrate. Helium ion scattering provides strong evidence that the oxygen is situated above the surface and in the <100> long bridge site. This is in agreement with results that have been obtained by several other groups [3,5,7,9,20]. On the other hand, Li^+ ion scattering data show no evidence of the shadowing of the substrate by the oxygen atoms, which would seem to indicate a subsurface position for the oxygen. This apparent discrepancy would appear to be due to the presence of oxygen-free copper atom rows, in the (2x1)-O structure whose scattering signal would tend to dominate. In the case of helium oxygen scattering, neutralization effects may reduce the importance of these oxygen-free rows.

Attempts to provide a clear conclusive evidence of the nature of the substrate reconstruction are not entirely satisfactory as none of the computer models for the proposed structures fully explains the experimental lithium angular spectra. The general consensus of published literature is that the missing row model correctly describes the oxygen induced reconstruction [3,4,6,8,10,11,12,16]. Generally, this missing row structure also describes our experimental results most accurately, although there remains one important discrepancy. The computer simulation predicts an extra peak in the polar angle scan in the <110> azimuth, which does not appear in the experimental data (trajectory c_{11}, figure 5.6). Theory suggests that this should be a strong feature, due to it being a simple shadowing event with no complicating multiple scattering, but no such feature is seen. The origin of this discrepancy is unknown.

5.3.1. Introduction to Cu(110)(2x3)–N

In the previous sections it was shown that adsorbates are capable of causing surface reconstruction, and there are many examples of both adsorbate–induced and clean surface reconstructions leading to overlayers exhibiting substantially larger periodicities than that of the clean surface structure [7,38,39]. For these structures it is recognised that it is unlikely that the long range periodicity is due to long range interactions, but that it is more likely to be the result of a coincidence between smaller, rationally related, meshes [7,23]. These adsorbate–induced reconstructions often have a similar structure to a related bulk compound [22,30].

The adsorption of oxygen and nitrogen leads to the formation of many similar structures on the various crystallographic planes of copper and nickel, [22,23,24,33 – 39]. It is a natural progression to study the adsorption of nitrogen on Cu(110) which forms the same LEED pattern as that obtained for nitrogen adsorption on Ni(110), viz. a (2x3) structure. Ion scattering is capable of providing detailed information concerning the surface structure, though in reality it has proved more useful in determining the substrate reconstruction. It is this substrate structural sensitivity of Li^+ ion scattering which we apply to try to establish whether surface reconstruction has taken place, as suggested by Heskett [22], or if it is simply a distorted ideal structure as proposed by Y. Kuwakara for Ni(110) [23]. We have, however, seen that in the case of Cu(110)(2x1)–O that the complementary use of He^+ can help to locate the adsorption site of light adsorbates

As we show below, the lithium ICISS data presented here exhibit many changes for the nitrogen dosed surface compared to the clean and the oxygen dosed surfaces. There is clear evidence that the surface has undergone a major reconstruction in passing to the Cu(110)(2x3)-N structure and the ICISS provides strong indications as to the nature of the reconstruction. In addition, the qualitative features of the helium

scattering data indicate that the nitrogen adsorbate is approximately coplanar with the surface copper atoms and sits in a local four fold hollow in the reconstructed top copper layer.

5.3.2. Results for Cu(110)(2x3)–N

This series of experiments was carried out using the same apparatus and the same Cu(110) sample which were used for the study of the adsorption of oxygen. Unlike oxygen, molecular nitrogen does not react with copper. To overcome this investigators have used several different methods to produce a chemisorbed nitrogen phase on copper. One route is to form atomic nitrogen which then reacts with the copper, [26,27] and this can be achieved by using electron bombardment in a nitrogen atmosphere, [23,24,25]. An alternative is to implant nitrogen by ion bombardment at energies ranging from 200 eV to 2 keV and then to anneal the surface [22,30]. In this investigation a variation of Heskett's ion bombardment method [22] was used. Specifically, the sample was ion bombarded at ≈2keV using a nitrogen pressure of≈$5x10^{-5}$ mbar, and then annealed at ≈550 K briefly to remove surface damage caused by the ion bombardment and produce the ordered chemisorbed nitrogen overlayer. The ion scattering data were taken in the principle azimuths, namely <100>, <110>, <211> and <111>, using exactly the same method used in the previous lithium ion scattering experiments on Cu(110) and Cu(110)(2x1)–O described above. The $Li^+ \rightarrow N$ scattering event could not be seen, but scattering from the nitrogen could be detected using helium ions. This $He^+ \rightarrow N$ scattering event has a weak scattering signal forcing the adoption of the multichannel data collection scheme, (see section 4.3). This means that the $He^+ \rightarrow N$ data were integrated over a fixed energy window for each angle of incidence, whereas the $Li^+ \rightarrow Cu$ data were collected in the single channel mode.

In figure 5.9, the lithium scattering angular scans obtained are compared with those obtained for Cu(110)(2x1)–O and from the clean Cu(110) surface. It can be seen that there are large changes in the angular scans compared to those from both the

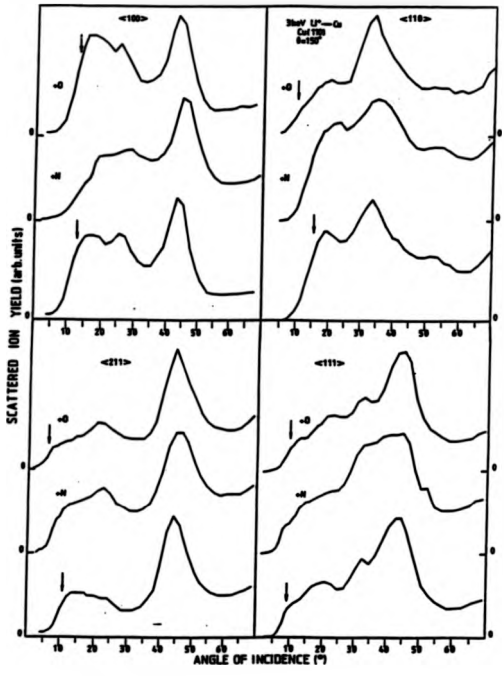

Figure 6.9 Plots of the dependence of the 3keV 150° $Li^+ \rightarrow Cu$ scattering signal as a function of grazing incidence angle in four principle azimuths from clean Cu(110), Cu(110)(2x1)-O and Cu(110)(2x3)-N. The arrows indicate the surface threshold angles corresponding to the (known) surface periodicities of the clean surface and the oxygen-induced reconstruction; these are <100>,3.61Å; <110>,2.55Å (clean), 5.11Å (+O); <211>, 4.42Å (clean), 8.84Å (+O); <111>, 6.63Å.

clean and the oxygen dosed surface. The various surface threshold positions are tabulated in table 5.1 and compared with the clean surface. Only one azimuth has maintained its clean surface atomic spacing, that is the <110> azimuth. Curiously both the <100> and the <111> azimuths appear to show two different surface thresholds. In the former there appears to be the presence of an atomic spacing close to that of the clean surface (3.4±0.1Å compared to 3.61Å) superimposed upon a larger grazing incidence peak corresponding to a shortening of the atomic spacing to (2.7±0.1)Å. The discrepancy of the first value from the bulk layer spacing is probably due to the disturbing influence of the latter feature. Heskett et al. [22] suggest that the nitrogen is adsorbed in the <100> long bridge site coplanarly, and a possible interpretation of the data might be that the shorter distance is due to nitrogen atoms shadowing the copper surface atoms. However, this adsorbate shadowing would not explain other azimuthal changes. In the <111> azimuth we have the two surface thresholds, corresponding to a spacing close to the clean surface, namely ((5.7±0.3)Å compared to 6.62Å), and to a longer spacing, namely (8.5±0.3)Å. The remaining <211> azimuth has only one surface threshold, though it exhibits a longer atomic spacing than for the clean surface (6.4Å compared to 4.42Å).

The lower layer features also exhibit significant changes. The most noticeable is that the angular features have been broadened, and this is most prominent in the <111> and the <110> azimuths. In the <111> azimuth there is now a broad peak covering the angular positions once occupied by two features, which were previously ascribed to out of plane scattering, the changes here maybe related to a reconstruction of the surface, though they cannot be modelled easily. Generally, there is a smearing of features in this azimuth not seen in the data for the oxygen covered surface. In the <110> azimuth the sublayer feature, has also become less prominent and has become broader. In the <211> and <100> azimuths only the smaller grazing angle events have been broadened, on the clean surface these were due to multiple scattering events down to the 2nd and the 3rd layers respectively. By contrast, the broad feature near the surface threshold in the <211> azimuth has become narrower, in a fashion similar to

Azimuth	Cu(110)		Cu(110)(2x3)-N	
	Angle(°)	Spacing(Å)	Angle (°)	Spacing(Å)
<100>	13¼	3.61	13¾	3.4
			15¾	2.6
<110>	15¾	2.55	16	2.55
<111>	9¼	6.26	10	5.7
			6½	8.5
<211>	11	4.42	9	6.4

Table 5.1 A table comparing the surface thresholds obtained using 3 kev Li^+ ions scattering through 150° from the Cu atoms in the Cu(110) and Cu(110)(2x3)-N surfaces.

that seen for the oxygen dosed surface (an effect which was attributed to the occurrence of the missing row reconstruction of the surface).

For helium scattering from the copper atoms (for which discernable surface thresholds have been obtained for the clean surface), the surface thresholds obtained from the nitrogen dosed surface are gentle slopes; by contrast the oxygen dosed surface data exhibited sharp surface thresholds (figure 5.10). On the other hand, the helium scattering from the nitrogen adsorbate exhibits very sharp surface thresholds in both the <100> and <110> azimuths, see figure 5.11. The usual explanation for the loss of threshold clarity in He^+ ion scattering angular scans is that there is increased neutralization due to the adsorbates. Here, the $He^+ \rightarrow N$ spectra clearly do not show this effect.

5.3.3. Structural Models for Cu(110)(2x3)–N

The changes in the apparent Cu–Cu distances in the surface inferred from the Li^+ ion scattering show that substrate reconstruction is occurring, and demonstrate that it does not involve a simple integral multiple of the atomic spacing commensurate with a (2x3) reconstruction.

A structure suggested by Kawahara for the Ni(110)(2x3)–N surface involves small atomic displacements of Cu atoms parallel to the surface and so is strictly a reconstruction model, figure 5.12. In this structure the nitrogen is assumed to be located in the <100> long bridge site, as proposed also by Heskett [22]. This leads to a structure with bond lengths and coordination close to the those of bulk compound copper nitride if the N and Cu top layer are nearly coplanar. To account for the shortened 2.7Å atomic spacing in the <100> azimuth seen in the data, however, the Cu atoms displacements would have to be of the order of 0.4Å. There are several points that mitigate against this structure. Firstly in the <100> azimuth there now exists three atomic spacings, namely 2.7Å, 3.61Å and 4.01Å and the latter would be expected to lead to a shift in the surface threshold towards more grazing angles of incidence. In

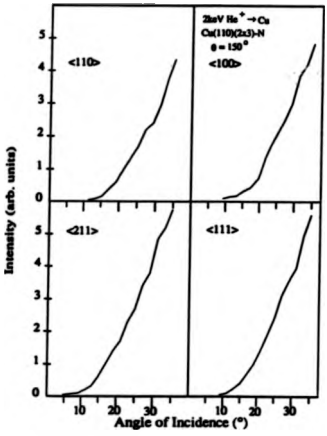

Figure 5.10 Plots of 2keV 150° He^+ ion intensity modulation as a function of the angle of incidence from copper atoms within the Cu(110)(2x3)–N surface in the four primary azimuths.

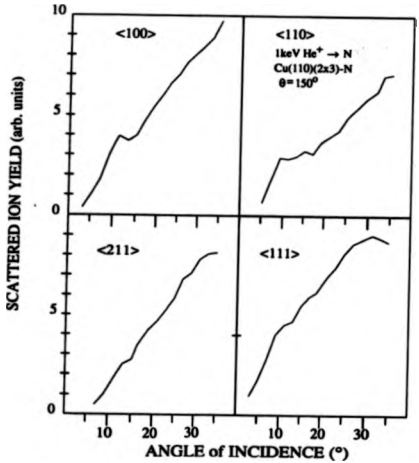

Figure 5.11 Plots of the dependence of the 2keV 150° $He^+ \rightarrow N$ scattering signal as a function of grazing incidence angle in four principle azimuths recorded from a Cu(110)(2x3)-N surface.

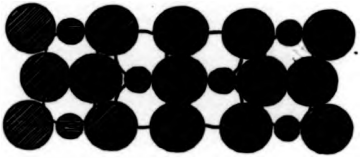

Figure 5.12 Y.Kuwahara et al. proposed structure for Ni(110)(2x3)-N surface based on the N occupation of the <100> long bridge sites and incorporating some distortion of the top layer.

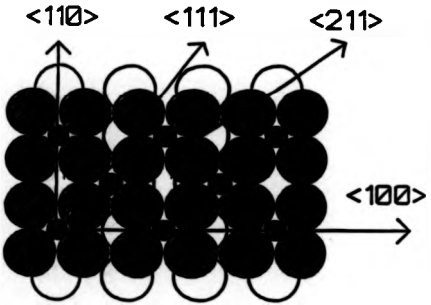

Figure 5.13 Schematic diagram of the proposed structure of Cu(110)(2x3)-N based on a reconstruction of the top Cu atom layer to a near-square mesh to produce a surface layer structure very similar to that of Cu(100)c(2x2)-N.

addition, the <110> surface threshold would shift by approximately 2½° due to out-of-plane scattering, and there would also be influences on the data in the other two azimuths. For the $He^+ \rightarrow N$ scattering event the siting of the nitrogen in the long bridge site would lead to a marked reduction in the scattering signal in the <100> azimuth at small grazing angles, an effect which was seen for the adsorption of the oxygen atoms in the long bridge site but is not seen in the data. Finally, it must be noted that if these large (≈0.4Å) lateral shifts of Cu atoms were to occur, the Cu-N bondlength would become much larger than in Cu_3N. This model also gives no clue as to why a (2x3) structure is formed.

A different model, proposed by D.P. Woodruff, is depicted in figure 5.13 [38]. In this structure the copper and nitrogen form an overlayer which is almost identical to the Ni(100)c(2x2)-N structure [24]. The close agreement of the 4<100> to 3<110> spacings provides an explanation for the (nx3) periodicity. Additionally the (2x3) structure can be seen as a need to produce a local c(2x2) square mesh, seen for many adsorbate systems [31,32,33,35,36], and associated with this, the exclusion of nearest neighbour hollow site filling by the nitrogen adsorbate. For this structure the <110> lattice spacing is identical to the clean surface value and the <100> spacing is reduced to 2.7Å. Both of these values are in accordance with the values deduced from the experimental $Li^+ \rightarrow Cu$ scattering data, though the perfect agreement with the latter must be seen to be rather fortuitous. In the other two azimuths the interpretation is difficult, since the experimental directions are not aligned with simple low index directions in the overlayer mesh. Strictly the periodicities in the <211> and <111> azimuths are 13.3Å and 18.8Å respectively, but there will be significant shadowing effects due to out of plane scattering. Close to the <211> azimuth the nearest atom is situated at 3.7Å, and using simple shadowing arguments and a knowledge of the shadow cone widths we find that this would produce a surface threshold at approximately 9.3° in this azimuth, which compares well with the experimental value of (9.0±0.5)° - this is again surprisingly good agreement with experiment.

Close to the <111> azimuth the nearest atoms are situated at 3.7Å and 5.79Å.

Using a similar analysis to that described for the <211> azimuth, a surface threshold position of approximately 5.8° is predicted. In the <111> and the <211> azimuths the experimental values agree with the theoretical values, but the theoretical values are subject to a large uncertainty, ~±1°.

Notice in figure 5.11 that the $He^+ \rightarrow N$ scattering intensities have similar values in all of the four azimuths near the surface threshold. This equality can only be obtained by placing the nitrogen atoms in the four fold hollow site, which allows maximum accessibility in all the azimuths. This positioning of the nitrogen atoms will produce surface thresholds (from N–N scattering) in the <110> and the <100> azimuths at similar angles to those seen in the experimental data. Indeed, surface threshold angular positions predicted on this basis agree rather well with the experimental values, although the effects of the neutralization introduces additional uncertainty. The diffuse nature of the intensity cut–offs in the other azimuths are consistant with the fact that the nitrogen atoms are not situated in simple rows along these clean surface azimuths, due to the locally incommensurate nature of the reconstruction, and the cut–off is probably dominated by neutralization effects.

In the reconstruction model the broadening and shifting of the sublayer $Li^+ \rightarrow Cu$ scattering events can be attributed to the shadowing and blocking of several symmetrically inequivalent sites for the surface layer relative to the subsurface layers. This complex structure, however, would require a more sophisticated modelling program and may added significantly to the information obtained.

5.3.4. Conclusions for Cu(110)(2x3)–N

The ion scattering data obtained indicate that a major adsorbate induced reconstruction of the surface layer occurs, with the $Li^+ \rightarrow Cu$ scattering data providing clear evidence for a distorted square lattice comparable to that of the Cu(100)c(2x2)N structure. In particular it predicts a large lateral motion of the <110> rows. Support for the nitrogen sitting in the four fold hollow is obtained from the $He^+ \rightarrow N$ scattering

results, which also exclude the <100> long bridge site. These conclusions are at variance with the suggestion of refs. 22&23 which both propose a long bridge site for the nitrogen (though both also suggest that a surface reconstruction is involved) but neither of these studies provided any quantitative evidence to support these suggestions. Although surprising, the formation of a square mesh metallic overlayer symmetry on a substrate of different symmetry is not unique; for example refs. 31&32 describe a structure in which sulphur causes a similar effect on the Ni(111) surface.

5.4. References

1. R.Fiedhans'l and I.Stensgaard, Surface Science **133** (1983) 453
2. A.G.J.Dewit, R.P.N.Bronkers and J.M.Fluit, Surface Science **82** (1979) 177
3. U.Döbler,K.Baberschke,J.Haase & A.Puschman, Phys. Rev. Lett. **52** (1984) 1437
4. E.Van de Riet, J.B.J.Smeltz, J.M.Fluit and A.Niehus, Surface Science **214** (1989) 111
5. R.P.N.Bronkers and A.G.J.Dewit, Surface Science **112** (1981) 133
6. J.Lapujoule, Y.Le Cruër, M.Lefort, Y.Lejay and E.Maurel, Surface Science **118** (1982) 103
7. G.R.Gruzalski,D.M.Zehner & J.F.Wendelhen, Surface Science **147** (1984) L623
8. J.Lapujoule, Y.Le Cruër, M.Lefort, Y.Lejay and E.Maurel, Phys. Rev. B **22** (1980) 5740
9. A.W.Robinson, J.S.Somers, D.E.Ricken, A.M.Bradshaw, A.I.D.Kilcoyne, D.P.Woodruff, Surface Science **227** (1990) 237
10. U.Döbler, K.Baberschke, D.D.Vvensky and J.B.Pendry, Surface Science **178** (1986) 679
11. H.Niehus and G.Comsa, Surface Science **140** (1984) 18
12. J.A.Yarmoff, D.M.Cyr, J.H.Huang, S.Kim and R.S.Williams, Phys. Rev. B **33** (1986) 3856
13. M.J.Ashwin and D.P.Woodruff, Vacuum **38** (1988) 291
14. R.Souda, M.Aono, C.Oshima, S.Otani, and Y.Ishizawa, Nucl. Instr. and Meths. **B18** (1986) 138
15. R.Countha, B.Cord, H.Wern, H.Saalfeld and S.Hüfner, Solid State Comm. **63** (1987) 619
16. M.Bader, A.Puschmann, C.Ocal and J.Haase, Phys. Rev. Lett. **57** (1986) 3273
17. J.C.Boulliard and M.P.Sotto, Surface Science **182** (1987) 200
18. W.Jacob, Appl.Phys. A. **41** (1986) 145
19. F.H.P.M. Habraken, P. Hofmann, S.Hachicha and A.M.Bradshaw, Surface Science **88** (1979) 285
20. H.P.Bonzel and S.Ferrer, Surface Science **118** (1982) L263

21 J.M. Mundenar, A.P. Baddorf, E.W.Plummer, L.G.Sneddon, R.Didio and D.M.Zehner, Surface Science **188** (1987) 15

22. D.Hesketh, A.Baddorf and E.W.Plummer, Surface Science. **195** (1988) 94

23. Y.Kuwahara, M.Fujisawa, M.Onchi and M.Nishijima. Surface Science **207** (1988) 17

24. H.C.Zeng, R.N.S.Sodhi and K.A.R.Mitchell, Surface Science **188** (1987) 599

25. R.E.Kirby, Surface Science **97** (1980) 457

26. G.G.Tibbets, J.H.Burkstrand and J.C.Tracy, Phys. Rev. **B15** (1977) 3652

27. G.G.Tibbets, J. Chem. Phys. **70** (1979) 3600

28. J.M.Burkstrand, G.G.Kleiman, G.G.Tibbet and J.C.Tracy, J.Vac. Sci. Technol. **13** (1976) 291

29. S.Ferrer, J.M.Rojo, Solid State Comm. **24** (1977) 339

30. M.Grunze, R.K.Driscoll, G.N.Burland, J.C.L.Connish and J.Pritchard, Surface Science **89** (1979) 381

31. T. Edmonds, J.J. McCarroll and J.Haase, Phys. Rev.Lett. **57** (1986) 3273

32. D.R.Warburton, P.L.Wincott, G. Thornton, F.M.Quinn and D.Norman, Surface Science **211/212** (1989) 71

33. S.Kono, C.S.Fadley, N.F.T.Hall and Z.Hussain, Phys.Rev.Letts. **41**(1978) 117

34. J. Stohr, R.Jaeger, S.Brennan, Surface Science **117** (1982) 503

35. E.Wimmer, C.L.Fu and A.J.Freeman, Phys.Rev.Letts. **55** (1985) 2618

36. T.S.Raham, D.L.Mills, J.E.Black, J.M.Szeftel, S.Lewald and H.I.Bach, Phys. Rev. **B30** (19840 589

37. M.Hock and J.Kippers, Surface Science **189** (1987) 575

38. M.J.Ashwin and D.P.Woodruff, submitted to Surface Science

39. A.W.Robinson, D.P.Woodruff, J.S.Somers, A.L.D.Kilcoyne, D.E.Ricken and A.M.Bradshaw, submitted to Surface Science

Chapter 6.
Alkali Adsorption on Cu(110)

6.1. Introduction

It is well known that adsorption of alkali metals on a surface reduces the work function by several eV [1,2,3], a fact made use of in the production of high efficiency photo and thermionic electron emitters [2]. Their use as activity promoters or modifiers for catalysts also provides a driving force for understanding the electronic structures of alkali adsorbed surfaces [1,2]. The widely held view is that for alkali coverages less than about 0.25 of a monolayer, the alkalis produce a strong reduction in work function due to charge transfer, but at greater concentrations depolarization leads to the formation of a metallic overlayer. This change in work function and eventual conversion from an ionic to a metallic overlayer is due to dipole interactions of the alkali and the surface, caused by charge transfer to the surface [1,3,10].

If we consider a singly charged alkali ion approaching a surface, its ionized state energy level broadens and increases in potential energy [8,14], figure 6.1. For alkali ion scattering neutralization occurs by resonant neutralization, see section 2.3.3. Assuming that the ion's broadened ionized level straddles the Fermi level, the fraction of the states in this level overlapping the filled energy states of the metal surface in potential energy will decrease with the increasing potential energy of the ion's ionized state. Consequently, the extent of electron exchange in equilibrium will decrease between the ion and the metal surface. If an alkali is adsorbed on the metal surface, the work function will decrease and therefore the overlap of the ion's ionized level and the filled states of the metal should increase; this will lead to an increasing fraction of the ion's unoccupied states being occupied. This will have the effect of reducing the ion fraction of the scattered flux.

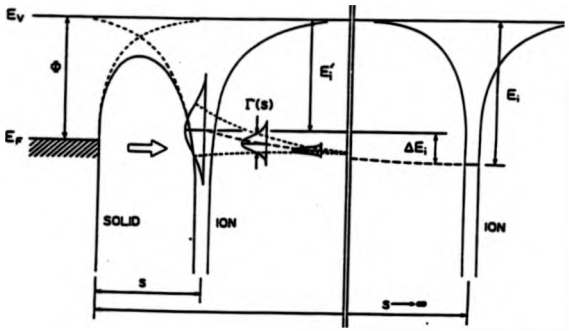

Figure 6.1 The energy levels of an ion and a solid target as the distance between them decreases. (M.Aono and R.Souda Nucl. Instr & Meths **B27** (1987) 55)

Our initial aim was to utilize Li^+ ions to see if this expected change in scattered ion charge fraction could be detected when alkali metals were adsorbed on the surface. Additionally, it is known that the work function of the alkali dosed surface typically passes through a minimum [1,3,4], and this could lead to a minimum in the ion fraction. At low coverages of alkali metals it is not clear whether the charge exchange process will be influenced by the average work function, or by the change in the local potential close to the adsorbate–substrate dipoles. We might hope to distinguish these by observing changes in the $Li^+ \rightarrow$adsorbate and $Li^+ \rightarrow$substrate scattering signals as a function of alkali adsorbate coverage. In the case of noble gas ions, neutralization proceeds via an Auger process and due to their deep ionization levels (which are totally overlapped by, or below, the filled energy levels of the metal), the possibility of reionization is then expected to be negligible; we might therefore expect this charge transfer to be unaffected by a change in the work function of a few eV.

In this investigation 1keV He^+ and Li^+ ion scattering were used to compare the effects of the alkali adsorption. Three alkalis were used, they were Na, K and Cs. Our LEIS studies of these surfaces reveal significant effects for both Li^+ and He^+ ion scattering which we associate with changes in charge transfer between the scattered ion and the surface due to changes in the surface's electronic structure. In particular, one normally observes in helium ion scattering that there is no inelastic background in the energy distribution, but we found that the alkalis induced the production of a significant inelastic background. One possible interpretation of this observation is that it may be due to the changes in the reionization probability of the helium neutrals [13].

A further feature of alkali metal adsorption on some (110) f.c.c. metal surfaces is the formation of a (1x2) [1,3,4,9] when a small amount of alkali adatoms (<0.1 of a monolayer) is present. The low coverage required to produce the LEED pattern characteristic of the reconstruction rules out the existence of a (1x2) structure based on adsorbate atoms alone [4,5]. It is thought that charge transfer from the alkali adlayer shifts the energy balance of the surface sufficiently to cause it to reconstruct [1,3,4]. One of the original objectives of our Cu(110)/alkali ICISS study was to investigate this

reconstruction, but despite many attempts we were unable to prepare the reconstructed phase.

6.1.1. Results and Discussion

The adsorption of the alkalis was carried out at room temperature using well degassed SAES getter sources. Changes in the work function were monitored by a retarding field method as a means of providing approximate coverage calibration, but this proved rather unreliable due to instrument instability. Three different alkali metals were deposited, namely Na, K and Cs, on to the Cu(110) surface for known exposure times at room temperature. 1keV Li^+ ion scattering is insensitive to low Z adsorbates and so could only be used to investigate the scattering from the adsorbate in the case of Cs, since the elastic scattering peak of Cs is situated well above the substrate elastic scattering peak in energy (and is therefore well away from the inelastic background).

For 1keV Li^+ ion scattering at an angle of incidence of 77° the variations of the intensities of the Cs and Cu elastic scattering peaks were monitored as a function of Cs adsorption time, and the results are presented in figure 6.2. The Cu elastic scattering signal exhibits a smooth decrease which could be due to adsorbate shadowing only. By contrast the Cs scattering signal does not exhibit a smooth increase, but shows a 'dip' in scattering intensity before saturation. When the spectral background was removed this 'dip' remained, indicating that the effect was not an artifact of the background. Note that although the abscissa of figure 6.2 is in terms of exposure, rather than coverage, a decrease in the sticking factor cannot account for a decrease in the scattered flux from the Cs adatoms. Moreover, if the effect is due to desorption of Cs, there should be an associated increase in the Cu scattering flux which was not seen. Hence, the trend does not seem to be a consequence of a change in the surface coverage. Elastic shadowing of the adlayer is also unlikely since Cs does not form multilayers at room temperature. A more likely explanation is that the result is evidence for a non-linear dependence of the charge fraction on the work function. The charge fraction is expected to decrease with decreasing work function due to the

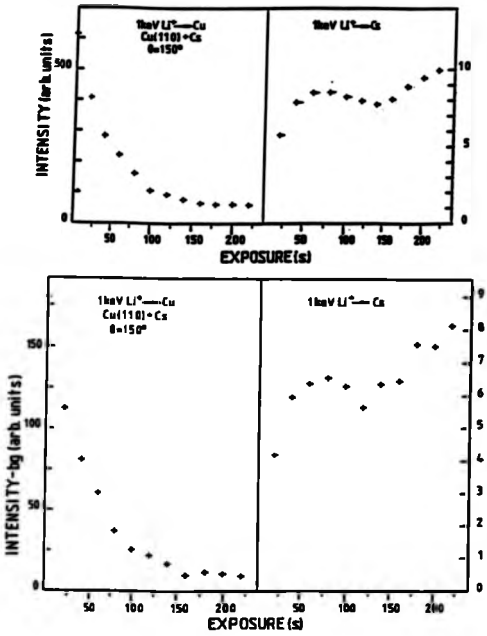

Figure 6.2 A plot of the variation of the Cu and Cs elastic peak intensities with increasing Cs exposure with and without the background, for 1keV Li ions undergoing a 150° scattering event for an incident angle of 77°.

increased overlap of the ionized orbital and the filled metal states [2]. Offset against this is a competing increase in the Cs scattering signal due to the increasing coverage. From figure 6.2 it appears that the decrease in scattered signal is due to the neutralization beginning to dominate over the increasing scattered signal beyond an exposure time of 125s, but thereafter the effect of neutralization decreases. It is known that there exists a minimum in the work function of alkalis [1,2,3,4], which should correspond to a minimum in the charge fraction, and the subsequent increase in scattering signal from the Cs adsorbate may be because the charge fraction is again increasing as the work function passes through this minimum.

The 'dip' in the Cs signal as a function of coverage is not matched by any similar effect in the Cu scattered signal. This suggests that the effects of a changing work function may have a less direct influence in the scattering of Li^+ from Cu, and that the attenuation of the scattered flux is dominated by adsorbate shadowing. Although we can account for the 'dip' in the scattered intensity from the Cs adatoms in terms of the change in the average work function, an alternative view of the charge exchange process is that the ions are sensing a change in the "local" work function in the vicinity of the alkali adatoms. This phenomenon has been used to account for results for the adsorption of Cs on W(100) in ref. [2], though only for coverages below 0.1 of a monolayer. It is known that for low alkali atom densities the adatoms are highly polarized [1] and that the associated dipoles remain relatively unchanged in magnitude up to a coverage close to that corresponding to the work function minimum [16]. For coverages greater than this the dipoles begin to depolarize each other and this ultimately leads to an increase in work function. If the incident ions sense the alkali atoms' local environment, then they will be influenced by this change in dipole moment. In this picture the charge fraction of an ion beam would be at a minimum when the dipoles are at their largest, and then it would increase with decreasing dipole moment, i.e. the detected ion intensity would increase. This would suggest that the neutralization would be most effective at low coverages, an effect not seen in the results; in fact the opposite occurs and suggests that the local work function picture is

not correct over the coverage range which we have studied.

Figures 6.3 and 6.4 show the variation in the intensity of 1keV He^+ scattering signals from Na, K and Cs adsorbed on Cu(110) collected at an incidence angle of 77°. The scattering from the three alkali adsorbates exhibits a similar behaviour to that seen for Li^+ ion scattering from the caesiated surface although the scattering signals are more nearly linear in exposure at low coverage. In the case of helium Auger neutralization is usually regarded as the main neutralization path, and might be expected to be relatively insensitive to changes of the work function by 2 or 3eV, since the helium 1s state is ≈20 eV below the Fermi level of the copper substrate [8]. It is also possible, however, for the 2s states of the helium ions to be involved in charge exchange. If these states are resonantly neutralized then the reverse process of resonant ionization is possible (Aono et al. [8] suggests that for TaC the reverse process has a probability of 1), but if the work function falls the balance will shift from resonance ionization to resonant neutralization, as is the case for lithium. Therefore, the form of the intensity plots, figures 6.3 and 6.4, in which there is is some suggestion of the 'dip' seen in the $Li^+ \rightarrow Cs$ data, may be a reflection of the change in charge fraction due to the change in the probability of the 2s states remaining neutralized; i.e. the addition of resonant neutralization to the existing Auger neutralization.

If the energy distribution curves for 1keV helium scattering off the alkali dosed surfaces are examined, figure 6.5, it can be seen that there is a background present at energies below the substrate and alkali elastic scattering peaks. Usually, for helium scattering of energies up to ≈5keV there is no background present. To obtain this background the helium ions must have undergone inelastic processes but still emerge from the surface in an ionized state. Normally helium ions have a greater probability of being neutralized if they have long trajectories in the solid as needed for substantial inelastic or multiple collisions; this results in the suppression of any background. If the observed background was due to direct scattering interactions with the alkali metal atoms only, it would not extend in energy up to the substrate elastic scattering peak for low Z alkali metal but would be lost above the alkali adsorbate elastic scattering peaks.

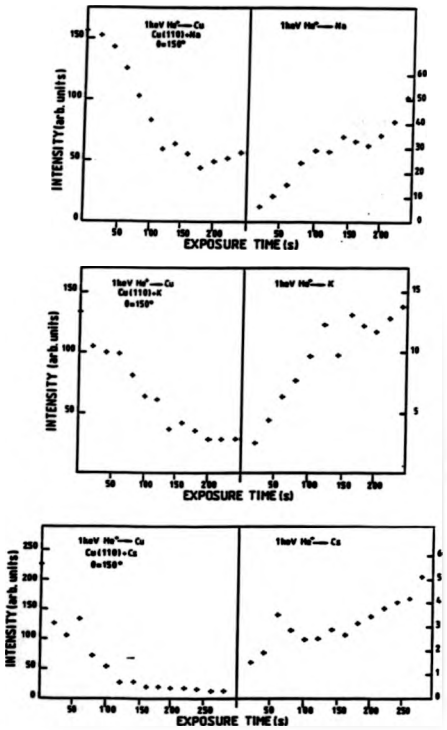

Figure 6.3 The variation in the intensity of the 1keV 150° He^+ ion scattering elastic peaks for the adsorbed alkalis and the copper substrate with increasing alkali exposure time.

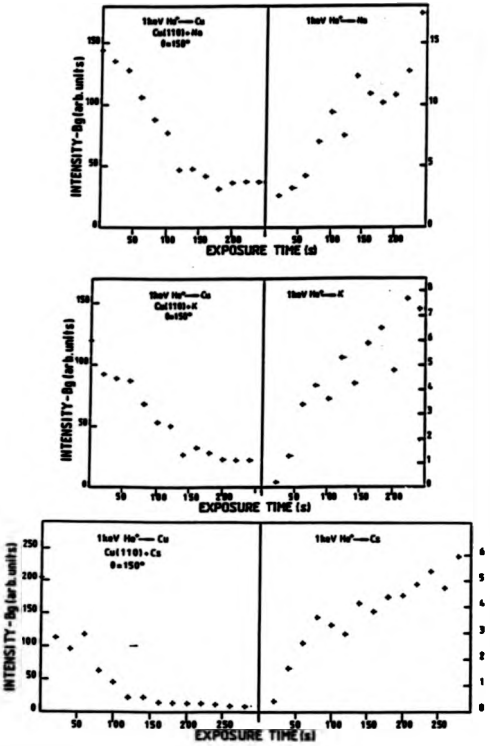

Figure 6.4 The variation in the intensity of the 1keV 150° He^+ ion scattering elastic peaks with background subtraction, for the adsorbed alkalis and the copper substrate with increasing alkali exposure time.

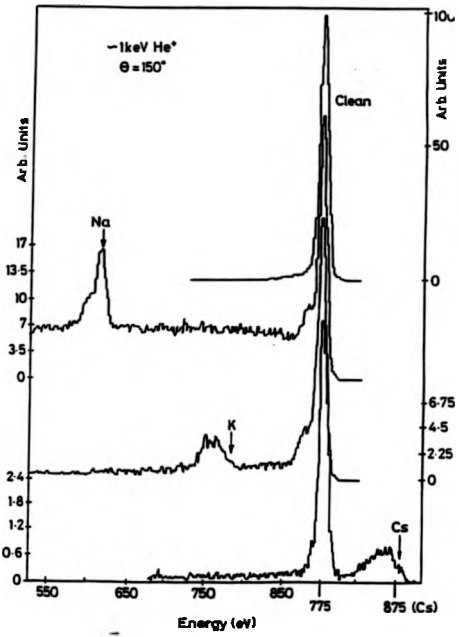

Figure 6.5 He^+ ion scattering spectra from a clean Cu(110) surface and from the same surface with sub-monolayer coverages of Na,K and Cs. The upper three spectra are recorded with a primary energy of 1100eV while the bottom spectrum was collected with a primary energy of 980eV. All spectra involved the same scattering angle of 150°

The results show that the background continues up to the substrate elastic scattering peak. The presence of this inelastic background between the low Z alkali and substrate elastic scattering peaks indicates that the ions and neutrals returning from the Cu substrate undergo processes within the alkali adlayer which enhances the probability of the helium remaining in an ionized state even after substantial energy losses. If the ions were to undergo weaker trajectory independent neutralization in the presence of the alkali metal adsorbate, then this would form an inelastic background, though this would tend to still increase the neutralization with increasing inelastic loss. This is not seen in practice; in fact the intensity of the background across the energy range is almost constant. Additionally, the alkali elastic scattering peaks in the energy distribution are wider than expected (compare with the Cu elastic scattering peak), and the predicted peak positions lie on the high energy side of these alkali elastic scattering peaks. Two possible reasons for these phenomena are 1) the neutral atoms emerging from the substrate are reionized [13] or 2) elastically scattered ions returning from the substrate are undergoing inelastic losses with a reduced neutralization probability [11] within the alkali adlayer.

Research into the possibility of reionization of helium neutrals has been carried out experimentally by Aono et al. [6,7,8] and theoretically by Tsukada et al. [10] for a range of materials. It is found that for helium kinetic energies up to 2keV Cu is unlikely to cause reionization, but Na and K are able to cause reionization for incident particle energies greater than ≈200eV. The mechanism is believed to be due to the interaction between the helium 1s state and the unfilled orbitals of the substrate near the Fermi level, but only during violent collision in which substantial electronic overlap occurs. In addition, if the trajectory is considered to be composed of three distinct parts (i.e. inward, collision and outward), it was found that the final charge state of the returning reionized ions is determined by charge exchange in the outward portion of the trajectory [6,7,8]. For the results presented here, this mechanism of reionization involving a violent collision could only account for the data if it was produced in $He^{+} \rightarrow Cu$ scattering events, and then only in the presence of the alkali

adsorbate. One feature of this reionization behaviour is that the elastic scattering peaks exhibit features that correspond to energy losses of ≈20eV, approximately the energy loss expected for the reionization of a ground state helium atom. Strangely, such a feature can be seen behind the $He^+ \rightarrow Cu$ scattering peak in the presence of the overlayer. From figure 6.5, it can be seen that the inelastic background is largest for Na and smallest for Cs, which is consistent with the trend of the alkali work functions. Within the collisional reionization model, however, there should be no dependence of reionization upon the work function.

One other possibility which avoids the postulation of a reionization mechanism, is that the elastically scattered ions undergo inelastic losses in the alkali metal overlayer only. This would then redistribute some fraction of the substrate elastic scattering peak intensity into an inelastic background at lower energies. For this to occur the neutralization probability in the overlayer would have to be much lower than in the copper. In the case of alkali metals, they form a highly polarized overlayer at low coverages and may have a lower neutralizing potential, since they have already donated electrons to the substrate. The processes involved may be a combination of inelastic collisions and electronic (mainly plasmon) losses [15]. At low alkali metal coverages the adlayer is highly polarized and therefore the electron density is lower compared to the metal, with increasing coverage the dipoles weaken and the electron density increases as the overlayer becomes more metallic in character. Hence, we would expect to see an increasing neutralization probability with increasing alkali metal coverage and therefore a suppression of the inelastic background. From the data it was noted that the background increased with increasing alkali metal coverage. Therefore the exact mechanism for a lower neutralization probability inelastic process is unclear.

In figure 6.3, it can be seen that the alkali metal elastic scattering peaks are broader than the clean surface copper elastic scattering peak, due to the appearance of lower energy shoulders. These shoulders are approximately 20eV lower in energy than the corresponding elastic scattering peak, similar to the ionization potential of the 1s

level of helium and appear to be due to the reionization of helium neutrals within the alkali adlayer [6,7,8]. In the case of K overlayers, additional broadening results from the fact that K does have two isotopes of atomic masses 39 and 41 which will produce elastic scattering peaks separated by 13eV. However, Tsukada et al. [10] states that reionization by Cu is unlikely for incident energies of less than 2keV, so this explanation is unlikely to account for the fact that the data presented here also show that the Cu substrate elastic scattering peak possesses a low energy shoulder in the presence of the overlayer.

6.1.2. Conclusions

The presence of an inelastic background in the 1keV helium energy distribution and the unexpected dependence of the He^+ and the 1keV Li^+ ion elastic scattering intensities on alkali coverages suggests that the alkali overlayer alters the probability of neutralization in both cases. The qualitative behaviour of charge fraction of the Li^+ ions scattering from the caesiated surface appears to be influenced by the average work function of the surface and not by local charges near the Cs adatoms. In particular, this would lead to the charge fraction decreasing more quickly than the increase in the Cs scattering signal due to increasing coverage which could account for the experimentally observed 'dip' in scattered signal. This effect is also seen in helium ion scattering for all three alkali metals adsorbed (Na,K and Cs) and is thought to be associated with additional resonance charge exchange. The appearance of an inelastic background in the helium ion scattering spectra for alkali overlayers may be due to a combination of an increased probability of reionization and inelastic losses within the alkali adlayer. Whether this is due to resonance exchange with the 2s levels, in a similar manner to lithium, or to the 1s level being reionized [8,10], is unknown.

6.1.3. References

1. T. Arunga and Y. Murato, Progress in Surface Science **31** 61
2. J.J.C.Geerlings, L.f.Tz.Kwakman and J.Los, Surface Science **184** (1987) 305
3. B.E.Hayden, K.C.Prince, P.J.Davie, G.Paolucci and A.M.Bradshaw, Solid State Comm., **48** (1983) 325
4. C.J.Barnes, M.Lindroos, D.J.Holmes and D.A.King, Surface Science **219** (1989) 143
5. H.P. Bonzel and S.Ferrer Surface Science **118** (1982) L263
6. R.Souda and M.Aono, Nucl. Instr. and Meths. **B15** (1986) 114
7. R.Souda, M.Aono, C.Oshima, S.Ontani and Y.Ishizawa, Surface Science **150** (1985) 459
8. M.Aono, R.Souda, Nucl. Instr. and Meths. **B27** (1987) 55
9. M.Copel, W.R.Graham, T.Gustafson and S.Yalisove, Solid State Comm. **54** (1985) 695
10. M.Tsukada, S.Tsuneyuki and N.Shima, Surface Science **164** (1985) L811
11. H.Niehus and E.Bauer, Surface Science **47** (1975) 222
12. H.H.Brongersma and P.M.Mul, Chem. Phys. Lett. **14** (1972) 380
13. M.J.Ashwin and D.P.Woodruff Vacuum **38** (1988) 291
14. S.H. Overbury, Nucl. Intr. and Meths **B27** (1987) 65
15. D.L.Seymour, C.F.McConville, D.P.Woodruff and J.E.Inglesfield, Surface Science **214** (1989) 57
16. A. Zangwill, Physics at Surfaces Cambridge University Press (1988)

Chapter 7.
Conclusions

The use of LEIS using the ICISS technique with a total scattering angle of 150° has yielded data for five different adsorbate systems, namely Cu(110)(2x1)-O, Cu(110)(2x3)-N, and the adsorption of the alkalis Na,K and Cs on Cu(110). In addition, information concerning the clean Cu(110) surface has also been obtained. To investigate the surface and subsurface atomic registry of the copper atoms, incident lithium ions were used, since they do not suffer trajectory dependent neutralization. Additionally, lithium displays a much lower neutralization rate with respect to helium (≈37% compared to ≈95%). One consequence of this trajectory independent neutralization is that the lithium ion energy distribution exhibits an inelastic background associated with lower layer scattering. This inelastic background was found to vary in intensity depending on the scattering condition, and in particular increased significantly with respect to the elastic scattering signal when a shadowing threshold occurred. It was found subsequently that the expected shadowing conditions in the ICISS regime could be reproduced most readily by taking the elastic scattering signal and the background together. Consequently, the scattering intensity modulations as a function of the angle of incidence were obtained by monitoring the total intensity of the elastic scattering, a single channel measurement, or by determining the area under this feature, a multichannel measurement. Using the former method, data were obtained for the clean and for the oxygen and nitrogen dosed Cu(110) surfaces. In addition, He^+ ion scattering was used to probe the scattering intensity from the low atomic mass adsorbates which could not be detected with Li^+ ions.

For the clean surface the data show evidence to support the theory of oscillatory *f.c.c.* interlayer spacing variations in the near surface region, though the expansion of the 2nd to 3rd layer spacing was larger than expected. For the oxygen dosed surface,

the results and subsequent computer modelling suggest that the surface has a missing row type reconstruction, though not all the details of the data are understood. In addition, the oxygen is confirmed as being approximately coplanar in the <100> long bridge site, conclusions which agree with the currently held view of at least some other researchers. A very different situation was found for the nitrogen dosed surface. Here, there was a large reconstruction of the surface in which the <100> azimuthal spacing was greatly reduced, thereby creating a distorted square mesh structure, similar to the Ni(100)c(2x2)-N surface. The nitrogen adsorbate resides in the new four fold hollow, with bond lengths close to those of the copper nitride compound.

In the final section a helium ion scattering study was carried out of the alkali adsorbate systems. For the alkali systems the effects of a change in the charge exchange process for He^+ on scattering manifested itself in the form of an inelastic background in the energy distribution. The reasons for this occurrence of an inelastic background do not appear to concur with current ideas concerning the neutralization and ionization processes. Additionally, the effect decreases with increasing alkali mass which also corresponds to decreasing work function at high coverages. The alkali elastic ion scattering peaks in the energy distribution exhibited wider peaks than expected, this is most likely due to reionization processes within the alkali adlayer. In the case of K there is also the additional effects of isotopes. These elastic peaks also do not follow the expected change in intensity with increasing adsorbate density, exhibiting a dependence which is not always increasing. This trend in the scattering intensity was also observed for the scattering of Li^+ from Cs and indicates that it is dependent on the average work function of the surface.

The results presented here solve some questions but also raise many more. For lithium ion scattering there is the problem of understanding the intensity of the scattered ion flux for some particular scattering events. The absence of scattering signal from low mass adsorbates is probably due to their smaller cross-sections compared to the substrate and to the influence of the large inelastic background, but this explanation does not account for unseen (but predicted) scattering trajectories

from the Cu(110)(2x1)-O surface. One way of investigating this problem might be to use another incident alkali ion, such as Na^+, for which published data suggest no such discrepancies exist. Alternatively, to reduce the complicating effects of both shadowing and blocking and of multiple scattering events, the scattering angle could be increased towards the ideal 180° (perhaps to the more usual 166°). The ideal route might be to follow the work of Aono et al. in ref. 1, in which a 180° scattering system has been developed, known as coaxial impact collision ion scattering spectroscopy (CAICISS). This offers many advantages, as outlined in ref. 1, if a fixed scattering angle is to be used. Principally it reduces the analysis to the simple shadow cone analysis outlined in chapter 2. In addition the time of flight approach allows one to detect neutrals as well as the ions.

The detection of helium neutrals would, moreover, prove useful in the examination of the alkali absorbed surfaces, coupled with reliable work function and alkali coverage measurements using helium ions as a probe. Here, the helium ion fraction could be determined directly and linked to the changes in work function. This may then provide information as to the reasons for the unexpected changes in the scattering intensities from the alkali absorbed surfaces. Hard information on the helium and lithium charge fractions from the clean and alkali dosed surface would certainly help to clarify the charge exchange processes occurring in these systems.

7.1. Reference

1. M.Aono, M.Katayama, E.Nomura, T.Chassé, D.Choi and M.Kato, Nucl. Instr. and Meths B37/8 (1989) 264

Chapter 8.
Appendices

Appendix A.

For the derivation of the standard binary collision, i.e. a process where the kinetic energy and momentum are conserved and there is no inelastic losses, figure 8.1.

Applying the conservation of energy, the energies before and after the collision can be related thus

$$E_o = E_1 + E_2 \qquad (1)$$

where

E_o = Energy of the incident ions

E_1 = Energy of the scattered ion

E_2 = Energy of the target atom after the collision

Considering the conservation of the momentum and resolving it into the components parallel and perpendicular to the original incident particle path, the following relationships hold

parallel $$m_1 v_o = m_1 v_1 \text{ Cos } \theta_1 + m_2 v_2 \text{ Cos } \theta_2 \qquad (2)$$

perpendicular $$0 = m_1 v_1 \text{ Sin } \theta_1 - m_2 v_2 \text{ Sin } \theta_2 \qquad (3)$$

rewriting these equations

$$m_1 v_o - m_1 v_1 \text{ Cos } \theta_1 = m_2 v_2 \text{ Cos } \theta_2 \qquad (4)$$

$$m_1 v_1 \text{ Sin } \theta_1 = m_2 v_2 \text{Sin } \theta_2 \qquad (5)$$

the equations are now squared and added together to form

$$(m_1 v_o - m_1 v_1 \text{ Cos } \theta_1)^2 + (m_1 v_1 \text{ Sin } \theta_1)^2 = (m_2 v_2)^2 \qquad (6)$$

which upon rearrangement and using the definition for the kinetic energy becomes:-

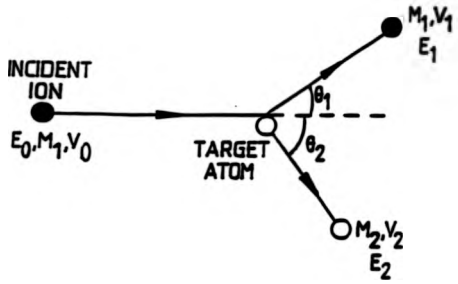

Figure 8.1 The scattering event utilized for determining theoretically the energy transfers during a binary collision, is depicted here and attributes the symbols used to the relevant particles.

$$m_1E_o - 2m_1(E_1E_2)^{1/2}\,\mathrm{Cos}\,\theta_1 + m_1E_1 = m_2E_2 \qquad (7)$$

using equation 1 and substituting in (7) for E_2 and dividing through by E_o the equation becomes

$$\left[1 + \frac{m_2}{m_1}\right]\frac{E_1}{E_o} - 2\left[\frac{E_1}{E_o}\right]^{1/2}\mathrm{Cos}\,\theta_1 + \left[1 - \frac{m_2}{m_1}\right] = 0 \qquad (8)$$

Solving for $(E_1/E_2)^{1/2}$ and letting $A = (m_2/m_1)$ then the equation becomes

$$\left[\frac{E_1}{E_o}\right]^{1/2} = \frac{1}{(1+A)}\,.\,[\,\mathrm{Cos}\,\theta_1 \pm [\mathrm{Cos}^2\theta_1 - (1+A)(1-A)] \qquad (9)$$

Which then transforms into the well known binary collision equation

$$\frac{E_1}{E_o} = \frac{1}{(1+A)^2}\,.\,[\,\mathrm{Cos}\,\theta_1 \pm (A^2 - \mathrm{Sin}^2\,\theta_1)^{1/2}\,]^2 \qquad (10)$$

From this equation we can see there is the possibility for two values for the ratio of E_1 to E_o in this section the the validity of only the positive sign for A>1 will be demonstrated.

If we allow A to equal 1 then the numerator of equation 9 becomes

$$\mathrm{Cos}\,\theta_1 \pm [\,\mathrm{Cos}^2\,\theta_1\,]^{1/2}$$

Therefore in this case only the positive sign will apply for A=1. To discover if both of the signs are valid either side of this value. Using the numerator of equation 9 and realizing that the energies are defined to be positive, then the following inequality can be obtained if only the positive sign is to be valid:–

$$\mathrm{Cos}\,\theta_1 < (A^2 - \mathrm{Sin}^2\,\theta_1)^{1/2} \qquad (11)$$

Hence

$$\mathrm{Cos}^2\,\theta_1 < A^2 - \mathrm{Sin}^2\,\theta_1$$

rearranging we obtain:–

$$A^2 > 1$$

or

$$A > 1$$

Therefore for values of A greater than 1 only the positive sign is valid.

Appendix B.

Using similar arguments and the same reference diagram a relationship is developed for the energy received by the target atom. Rearranging equations 2 and 3 in appendix A the following are obtained:–

$$m_1 v_o - m_2 v_2 \text{ Cos } \theta_2 = m_1 v_1 \text{ Cos } \theta_1 \qquad (1)$$

$$m_2 v_2 \text{Sin } \theta_2 = m_1 v_1 \text{ Sin } \theta_1 \qquad (2)$$

Now squaring these two equations and adding them together yields

$$(m_1 v_o - m_2 v_2 \text{ Cos } \theta_2)^2 + (m_2 v_2)^2 \text{ Sin}^2 \theta_2 = (m_1 v_1)^2 \qquad (3)$$

Using the definition of kinetic energy and substituting for E_1, equation 3 becomes:–

$$2(m_1 m_2)^{1/4} (E_o E_1)^{1/4} \text{ Cos } \theta_2 = (m_2 + m_1) E_2 \qquad (4)$$

Squaring and rearranging equation 4 yields the expected equation thus :–

$$\frac{E_2}{E_o} = \frac{4A \text{ Cos}^2 \theta_2}{(1 + A)^2} \qquad (5)$$

Appendix C

Using the binary collision formula developed in appendix A, this section will develop an expression for the mass resolution, $m_2 / \Delta m_2$, as a function of the detection ion energy resolution, $E_1 / \Delta E_1$. First let

$$B = (1 + A)^{-2} \text{ and}$$

$$C = [\text{Cos } \theta_1 + (A^2 - \text{Sin}^2 \theta_1]$$

then the equation becomes :–

$$E_1 / E_o = B \, . \, C^2$$

Differentiating this equation with respect to m_2 yields

$$\frac{1}{E_o} \cdot \frac{\delta E_1}{\delta m_2} = -2(1 + A)^{-3} \, . \, \frac{1}{m_1} \, . \, C^2 + 2 \, . \, B \, . \, C \, . \, (A^2 - \text{Sin}^2 \theta_1)^{-1/4} \, . \, A.m^{-1} \qquad (1)$$

Multipling both sides by m_2 and rearranging the equation yields the expected equation for the mass resolution –

$$\frac{m_2}{\delta m_2} = \frac{E_1}{\delta E_1} \cdot \frac{2A}{(1 + A)} \cdot \frac{A + \text{Sin}^2 \theta_1 - \text{Cos } \theta_1 (A^2 - \text{Sin}^2 \theta_1)^{1/4}}{A^2 - \text{Sin}^2 \theta_1 + \text{Cos } \theta_1 (A^2 - \text{Sin}^2 \theta_1)^{1/4}} \qquad (2)$$

TITLE **Low Energy He^+ and Li^+ Ion Scattering from Surfaces**

AUTHOR Mark John Ashwin

INSTITUTION and DATE University of Warwick 1990